

Mantle Xenoliths from Tenerife (Canary Islands): Evidence for Reactions between Mantle Peridotites and Silicic Carbonatite Melts inducing Ca Metasomatism

E.-R. NEUMANN^{1*}, E. WULFF-PEDERSEN^{2†}, N. J. PEARSON³ AND E. A. SPENCER²

¹DEPARTMENT OF GEOLOGY, UNIVERSITY OF OSLO, PO BOX 1047 BLINDERN, N-0316 OSLO, NORWAY

²MINERALOGISK–GEOLOGISK MUSEUM, SARSGT. 1, N-0562 OSLO, NORWAY

³ARC NATIONAL KEY CENTRE FOR GEOCHEMICAL EVOLUTION AND METALLOGENY OF CONTINENTS, DEPARTMENT OF EARTH AND PLANETARY SCIENCES, MACQUARIE UNIVERSITY, SYDNEY, NSW 2119, AUSTRALIA

RECEIVED APRIL 18, 2001; REVISED TYPESCRIPT ACCEPTED NOVEMBER 12, 2001

Mantle xenoliths from Tenerife show evidence of metasomatism and recrystallization overprinting the effects of extensive partial melting. The evidence includes: recrystallization of exsolved orthopyroxene porphyroclasts highly depleted in incompatible trace elements into incompatible-trace-element-enriched, poikilitic orthopyroxene with no visible exsolution lamellae; formation of olivine and REE–Cr-rich, strongly Zr–Hf–Ti-depleted clinopyroxene at the expense of orthopyroxene; the presence of phlogopite; whole-rock CaO/Al₂O₃ » 1 (Ca metasomatism) in recrystallized rocks; and enrichment in incompatible elements in recrystallized rocks, relative to rocks showing little evidence of recrystallization. The 'higher-than-normal' degree of partial melting that preceded the metasomatism probably results from plume activity during the opening of the Central Atlantic Ocean. Sr–Nd isotopic compositions are closely similar to those of Tenerife basalts, indicating resetting from the expected original mid-ocean ridge basalt composition by the metasomatizing fluids. Metasomatism was caused by silicic carbonatite melts, and involved open-system processes, such as trapping of elements compatible with newly formed acceptor minerals, leaving residual fluids moving to shallower levels. The compositions of the metasomatizing fluids changed with time, probably as a result of changing compositions of the melts produced in the Canary Islands plume. Spinel dunites and wehrlites represent rocks where all, or most, orthopyroxene has been consumed through the metasomatic reactions.

KEY WORDS: Canary Islands; Tenerife; mantle xenoliths; geochemistry; Ca metasomatism; open-system processes; lithosphere; ocean islands

INTRODUCTION

The combination of petrographic studies and analyses of the abundances of elements in mantle rocks and their minerals is essential for unravelling the evolutionary history of different parts of the lithospheric mantle. The evolution of methods for *in situ* trace element analyses in minerals has opened a new world of possibilities for information on the composition and evolution of the upper mantle. *In situ* trace element data on minerals have added very important information about, and understanding of, mantle processes, particularly mantle metasomatism and metasomatic agents (e.g. Salters & Shimizu, 1988; Johnson *et al.*, 1990; Vannucci *et al.*, 1991, 1993, 1998; Roden & Shimizu, 1993; Eggins *et al.*, 1998; Coltorti *et al.*, 1999; Glaser *et al.*, 1999; Griffin *et al.*, 1999; Garrido *et al.*, 2000; Grégoire *et al.*, 2000; Xu *et al.*, 2000). However, so far such data are available on minerals in mantle rocks from only a restricted number of

*Corresponding author. E-mail: e.r.neumann@geologi.uio.no

†Present address: Technoguide, A/S, Aslakveien 14, N-0753 Oslo, Norway.

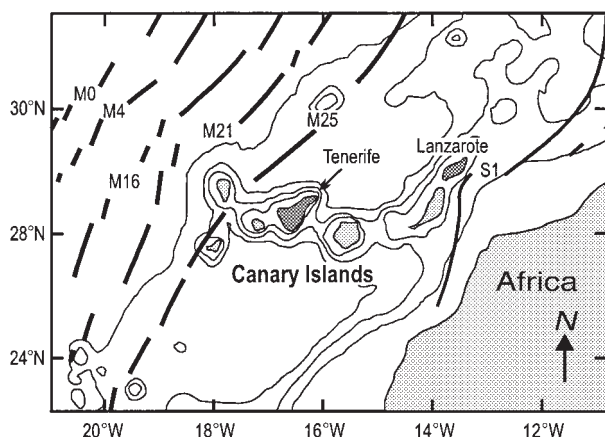


Fig. 1. Map of the Canary Islands showing bathymetry (with 1000 m contours) and magnetic anomalies [simplified after Verhoef *et al.* (1991) and Roest *et al.* (1992)].

localities, and the database for ocean islands is particularly restricted. More data are clearly needed.

The Canary Islands are located in the Magnetic Quiet Zone close to the coast of Africa (e.g. Verhoef *et al.*, 1991). The magnetic anomaly M25 passes the western Canary Islands, and anomaly S1 is located east of the easternmost islands (Fig. 1; Verhoef *et al.*, 1991; Roest *et al.*, 1992), indicating that all the Canary Islands rest on oceanic lithosphere of 150–170 Ma age. The oldest exposed volcanic rocks in the Canary Islands are ~20 Ma in Lanzarote, but decrease westwards along the island chain in age and are <4 Ma in La Palma (e.g. Abdel-Monem *et al.*, 1971, 1972; Schmincke, 1982). Studies of mantle xenoliths show that the upper mantle beneath the Canary Islands consists of highly depleted spinel peridotites that have been subjected to metasomatism (e.g. Neumann, 1991; Siena *et al.*, 1991; Neumann *et al.*, 1995; Wulff-Pedersen *et al.*, 1996). Mid-ocean ridge basalt (MORB)-type oceanic crust has been identified beneath Lanzarote, Gran Canaria and La Palma (Hoernle, 1998; Neumann *et al.*, 2000; Fig. 1). Former studies have shown that the type and extent of metasomatism vary among the Canary Islands (e.g. Johnsen, 1990; Neumann, 1991; Siena *et al.*, 1991; Neumann *et al.*, 1995; Wulff-Pedersen *et al.*, 1996), and preliminary results suggest that the metasomatism in the upper mantle beneath Tenerife is more intense, and may have a somewhat different character, compared with that beneath the other islands (Wulff-Pedersen *et al.*, 1999). The aim of this study is (a) to describe the petrographic and chemical character of the upper mantle beneath Tenerife on the basis of mantle xenoliths, (b) to present major and trace element data for bulk rocks and minerals in a series of mantle xenoliths from Tenerife, (c) to determine the nature of the processes that have been in operation in the upper mantle, and

(d) to identify the type of transport agent that has caused mantle metasomatism.

PETROGRAPHY

The data presented in this paper are on xenoliths with a diameter of ~5–15 cm, from locality TF14 in Montaña Roja, a cinder cone of ~750 ka age on the south coast, just SW of the small town El Medano. The xenoliths are dominated by spinel harzburgites and lherzolites, and are generally fresh. Mantle xenoliths have also been found in a basaltic dyke located east of Masca in the Teno Complex (NW Tenerife). These xenoliths, which are almost exclusively of spinel dunites and wehrlites, are small (a few centimetres in diameter) and strongly weathered, and are not discussed here.

Spinel harzburgites and lherzolites

Spinel harzburgite and lherzolite xenoliths from Tenerife are protogranular to porphyroclastic and consist of 70–91 vol. % olivine (ol), 6–26 vol. % orthopyroxene (opx), <2–9 vol. % clinopyroxene (cpx), << 1–3 vol. % spinel (sp) and << 1–3 vol. % glass. Two samples with >90 vol. % olivine are classified as harzburgites because they are rich in orthopyroxene and are texturally similar to the harzburgites and lherzolites. About half the samples contain trace amounts of phlogopite. Rare carbonates have been observed in some samples; those in interstitial domains consist of granular aggregates and appear to be secondary. However, magnesite and dolomite crystals in CO₂-rich fluid inclusions and in polyphase inclusions dominated by silicate glass appear to be primary. Modal olivine–orthopyroxene–clinopyroxene relationships (determined by point-counting several thousand points in each sample) are presented in Fig. 2.

The xenoliths exhibit two main types of texture that are primarily expressed in the appearance of orthopyroxene. We shall refer to these as HEXO (harzburgites exhibiting only strongly exsolved and deformed orthopyroxene porphyroclasts) and HLCO (harzburgites and lherzolites containing only 'clear' orthopyroxene porphyroclasts, i.e. without visible exsolution lamellae or deformation features). Harzburgites with transitional textures are referred to as HTR. Details are given below. All the lherzolites belong to the HLCO group (Fig. 2), which, in general, contain more olivine and clinopyroxene and less orthopyroxene than do HEXO and HTR (Fig. 2). Fluid inclusions are described briefly in connection with the various host minerals, but are discussed in more detail in a separate paper (Frezzotti *et al.*, 2002). Of the two samples with >90% olivine, one falls in the HEXO, the other in the HLCO group.

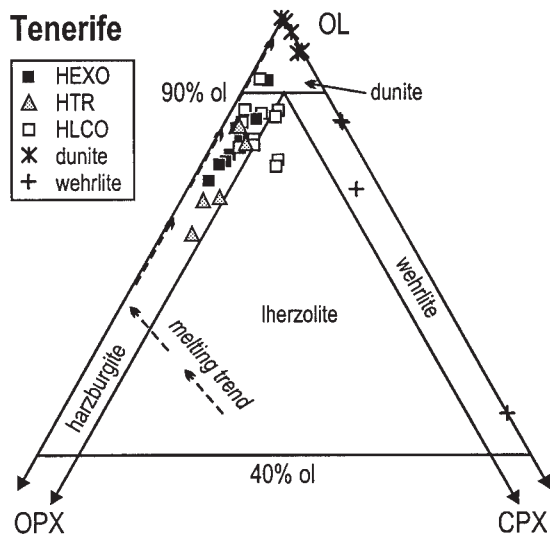


Fig. 2. Modal olivine–orthopyroxene–clinopyroxene relations in mantle xenoliths from Tenerife. HEXO, spinel harzburgite xenoliths with exsolved orthopyroxene; HLCO, spinel harzburgites and lherzolites with clear recrystallized orthopyroxene without exsolution lamellae; HTR, harzburgites with both exsolved and clear orthopyroxene. Dashed arrows show, in a generalized manner, the olivine–orthopyroxene–clinopyroxene relationships in mantle residues formed by progressive partial melting. The trends are based on partial melting experiments on fertile peridotite at upper-mantle pressures (Jaques & Green, 1980). The arrowheads point in the directions of increasing degree of partial melting. (See text for further discussion.)

Olivine in HEXO mainly forms strongly to moderately deformed porphyroclasts or medium-sized grains (≤ 5 mm long) cut by numerous inclusion trails dominated by CO_2 and/or silicate glass. Some CO_2 inclusions have a thin rim of silicate glass or talc–serpentine, with dolomite, magnesite, halite, sulphide, and phlogopite as daughter minerals. Less commonly olivine occurs as clusters of mildly strained to unstrained neoblasts (<0.5 mm) with interlocking grain boundaries. In HTR and HLCO olivine mainly forms deformed, medium-sized grains (<0.5 mm in diameter), but is also present as blebs or inclusions in clinopyroxene and in clear domains in orthopyroxene porphyroclasts; large blebs may exhibit undulatory extinction (Fig. 3c). Olivine neoblasts, particularly olivine blebs enclosed by orthopyroxene in HLCO, may contain linear rows of minute spinel inclusions.

Orthopyroxene in HEXO is mainly present as porphyroclasts of different sizes (up to 8 mm in diameter) with exsolution lamellae of clinopyroxene, or, less commonly, spinel. They show indications of strain in bent and broken exsolution lamellae (Fig. 3a), and are very rich in small CO_2 -rich fluid inclusions, silicate glass inclusions, and polyphase inclusions with silicate glass. Locally the porphyroclasts exhibit domains without visible exsolution lamellae. These domains are commonly associated with

secondary fluid inclusion trails and may contain rounded blebs or neoblasts of olivine and clinopyroxene. Clusters of subhedral neoblasts (<0.5 mm) of $\text{opx} + \text{cpx} + \text{ol} \pm \text{sp}$ or $\text{opx} + \text{ol} + \text{cpx}$ may be present along the rims of exsolved porphyroclasts. Large ‘clear’ orthopyroxene porphyroclasts (≤ 6 mm in diameter) in HLCO are commonly poikilitic, enclosing numerous rounded to irregular grains of olivine and clinopyroxene (<0.5 mm in diameter; Fig. 3b), clusters of irregular to vermicular spinel, and single, rounded to equant spinel grains. The ‘clear’ orthopyroxene grains show minor or no indications of strain, although coexisting olivine porphyroclasts are strained to the same degree as those in HEXO. Fluid or glass inclusions are very rare. The orthopyroxene in HLCO (and HTR) also forms small interstitial grains in neoblast areas, and blebs and irregular domains inside clinopyroxenes (Fig. 3c). The HTR show a gradual transition from exsolved orthopyroxene porphyroclasts very rich in fluid and glass inclusions with scattered exsolution-free domains, to large, ‘clear’, poikilitic orthopyroxene grains enclosing blebs of olivine and clinopyroxene without visible glass or fluid inclusions.

Clinopyroxene in HEXO is present as small, irregular neoblasts (generally <0.5 mm) along the boundaries of orthopyroxene porphyroclasts, and inside clear parts of orthopyroxene porphyroclasts (Fig. 3b), and may form separate, interstitial grains enclosing vermicular spinel. In HLCO (and HTR) clinopyroxene commonly forms poikilitic, anhedral grains (oikocrysts (≤ 2 mm in diameter) enclosing rounded neoblasts and blebs of olivine, blebs or irregular grains of orthopyroxene, and irregular to vermicular spinel (Fig. 3c). Domains exhibiting spinel exsolution lamellae are found locally in large grains. Clinopyroxene is also present in clusters of neoblasts ($\text{cpx} \pm \text{ol}$) enclosed by ‘clear’ orthopyroxene (Fig. 3b).

Spinel generally forms equant to vermicular grains (mainly <0.5 mm in diameter) enclosed by clinopyroxene, less frequently enclosed by poikilitic orthopyroxene or by olivine neoblasts. Rounded spinel grains are common along grain boundaries. In rare cases, spinel forms larger grains (up to 2 mm in diameter), crosscut by trails of glass or pyroxene.

Phlogopite is generally present in trace amounts in polyphase inclusions in olivine and exsolved orthopyroxene. However, one sample, lherzolite TF14-42 (HLCO), contains ~ 5 vol. % euhedral to subhedral phlogopite (≤ 1 mm). The phlogopite occurs in interstitial clusters of phlogopite (Fig. 3d) or phlogopite + clinopyroxene, and encloses blebs of olivine and orthopyroxene. Some of these clusters include large spinel grains criss-crossed by pyroxene-filled fractures. With the exception of sample TF14-42, we found no general difference between HEXO and HLCO with respect to the presence or absence of phlogopite.

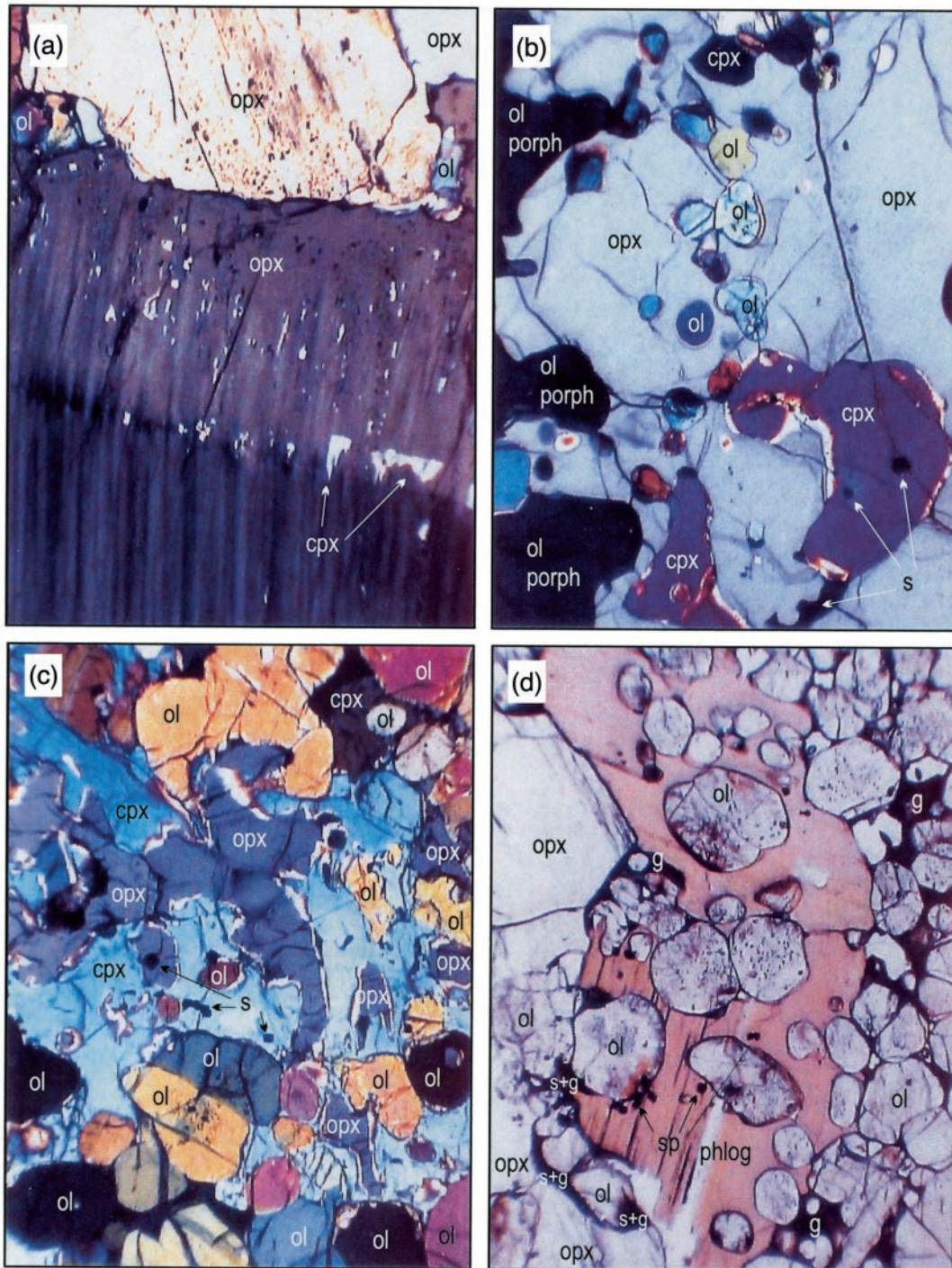


Fig. 3. Photomicrographs showing petrographic features of mantle xenoliths from Tenerife. Each photograph covers an area of about $1.5 \text{ mm} \times 2 \text{ mm}$. (a) Kinked orthopyroxene with clinopyroxene exsolution lamellae and fluid and solid inclusions; glass inclusions appear as small black spots; spinel harzburgite TF14-48 (HEXO). Crossed polars. (b) 'Clear' orthopyroxene enclosing rounded olivine blebs and clinopyroxene; spinel lherzolite TF14-36 (HLCO). Crossed polars. (c) 'Clear', poikilitic clinopyroxene enclosing irregular remnants of orthopyroxene and small, rounded olivine grains; spinel lherzolite TF14-59 (HLCO). Crossed polars. (d) Interstitial phlogopite next to 'clear' orthopyroxene, both enclosing small, rounded olivine grains rich in fluid and spinel inclusions; spinel harzburgite TF14-42 (HLCO). cpx, clinopyroxene; ol, olivine; opx, orthopyroxene; phl, phlogopite; s, spinel; g, glass; phen, phenocryst.

Silicate glass is present interstitially, as glass inclusions in mineral phases, and as polyphase inclusions (glass + CO₂ ± carbonates ± spinel ± phlogopite ± clinopyroxene) where silicate glass is the dominant phase. Glass inclusions and polyphase inclusions are particularly common in olivine and orthopyroxene porphyroclasts in HEXO, whereas in HLCO glass mainly occurs interstitially.

Spinel dunites

The spinel dunite xenoliths are granoblastic. In addition to olivine they contain 0.0–4 vol. % clinopyroxene, 1–2 vol. % spinel, trace amounts to 5 vol. % interstitial glass, and may contain trace amounts of phlogopite. Orthopyroxene (<1 vol. %) has been observed only in sample TF14-4.

Moderately deformed olivine is present in a range of grain sizes from ~7 mm to << 0.5 mm; the most common grain size is ~3 mm. With the exception of very small grains that are generally rounded to subhedral and commonly associated with glass, grain boundaries are highly irregular. Undeformed Cr-diopside (<2 mm) typically forms interstitial grains enclosing small, rounded blebs of olivine and vermicular or rounded spinel. Spinel is also found as rounded grains (≤1 mm) along grain boundaries, and as tiny, rounded inclusions in olivine. Orthopyroxene (TF14-4) forms intergrowths with Cr-diopside, blebs in olivine and Cr-diopside, and inclusions in olivine (opx ± cpx + silicate glass). Phlogopite is observed only as parts of polyphase inclusions in olivine. Fluid inclusions are uncommon.

Spinel wehrlites

Spinel wehrlites contain 41–85 vol. % moderately deformed olivine, 13–48% clinopyroxene, <1–8% spinel, and minor amounts of interstitial glass (<1–4%). One sample (TF14-46) carries ~3 vol. % poikilitic orthopyroxene; occasionally orthopyroxene blebs form inclusions in clinopyroxene. Some samples also contain trace amounts of phlogopite in polyphase inclusions in olivine.

Relatively olivine-rich wehrlites have similar textures to the dunites, but clinopyroxene and spinel grains are larger, and the poikilitic texture of the clinopyroxene is more strongly developed. Secondary fluid and polyphase inclusion trails are most common in olivine, whereas sulphide inclusions are small and relatively rare. In clinopyroxene-rich samples, clinopyroxene forms large (≤7 mm in diameter) grains with interlocking boundaries, locally containing numerous trails of polyphase fluid and sulphide inclusions. Olivine tends to form clusters of relatively small grains (<1 mm), although poikilitic grains

occur. Spinel (≤3 mm) generally forms rounded to irregular grains along grain boundaries, or is enclosed by clinopyroxene.

ANALYTICAL METHODS

Trace element analyses of minerals were obtained using the laser ablation microprobe (LAM) housed in the Geochemical Analysis Unit, GEMOC Key Centre, Macquarie University. The LAM used in this study is a custom-built UV (266 nm) laser microprobe coupled to an Agilent 7500s inductively coupled plasma mass spectrometry (ICPMS) system [described in detail by Norman *et al.* (1996)]. The laser was operated at a repetition rate of 10 Hz and typical energy of 0.5–1 mJ per pulse, allowing data collection from individual grains in polished thick sections (100 μm) for at least 100 s. Ar with a flow rate of ~1.5 l/min was used as the carrier gas. The Agilent 7500s was operated without the shield torch option, with a forward power of 1350 W, and tuned to give oxide production <0.5% (measured as Th:ThO). Data collection was monitored in time-resolved format and the data were processed on-line using GLITTER, a data reduction software package developed at GEMOC. The time-resolved signals were selectively integrated to ensure processing of the most representative portion of the ablation signal. This procedure allows anomalies in the signal to be assessed and interpreted using analytical and mineralogical criteria. Calibration was based on the NIST 610 trace element glass standard with reference values from Norman *et al.* (1996). Calcium was used as the internal standard for quantification of clinopyroxene analyses, magnesium for olivine and orthopyroxene. The calibration protocol involves standardization at the beginning, middle and end of each analytical run to correct for instrumental drift during the run. During each run the standard BCR2G was analysed as an unknown. The accuracy and reproducibility of the analyses are summarized in Table 1. Trace element data on minerals and glasses are reported in Tables 2, 4, 6 and 9. For elements occurring below the detection limit, the detection limit is indicated.

Minerals and glasses were analysed for major elements using a CAMECA CAMEBAX electron microprobe fitted with a LINK energy-dispersive system at the Mineralogical–Geological Museum in Oslo. Accelerating voltage was 15 kV and counting times were 10–30 s. Minerals were analysed using a beam current of 20 nA, and a focused beam, whereas glass analyses were performed with a beam current of 10 nA and the beam rastered over an approximately 10 μm × 10 μm area to minimize Na loss. Na data were acquired first to preclude any underestimation (Tables 3, 5 and 7–9).

Table 1: A compilation of data on BCR2G analysed as unknowns (normalized to NIST 610)

Source:	Solution ICPMS analysis					LAM-ICPMS				
	Memorial	Norman <i>et al.</i>		GEMOC		Norman <i>et al.</i>		Agilent 7500s Feb–Mar 2001		
				σ	$n = 40$	σ		σ	$n = 52$	σ
Li	9.98	9.6	0.5	7.90	0.33			9.67	0.84	8.7
Be				2.66	0.16			2.16	0.11	5.1
Be								9.1	3.7	40.7
Al								71.9	2200	3060
P								1256	99	7.9
Sc		33.5	0.4	33.86	0.44	33	0.8	32.2	1.0	3.1
Ti				13600	240			14090	550	3.9
V		429	7	396.5	4.5	414	8	419	12	2.9
Cr				16.69	0.58					
Co		38	1	36.45	0.52	35.8	1.3	35.8	1.6	4.5
Ni		13.3	0.3	13.46	0.43	10.8	0.7	11.23	0.62	5.5
Cu		34.1	1.2	27.2	1.4	19.4	1.0			
Zn		129	4	125.4	2.8	147	12			
Ga		21.9	0.5	21.15	0.32	22.7	0.9	22.2	1.5	6.8
Rb	47.51	48.1	0.9	46.42	0.93	49	2	49.6	2.4	4.8
Sr	336.8	335	7	329.1	5.3	342	6	346	10	2.9
Y	32.5	39.4	0.8	38.0	0.5	35	6	34.3	1.7	5.0
Zr	184	201	2	192.4	2.3	194.0	0.7	190	11	5.8
Nb	13.1	13.1	0.1	12.64	0.29	12.8	0.4	13.32	0.92	6.9
Mo	287	255	4	252	25	244	7			
Cs	1.19	1.18	0.01	1.192	0.044	1.13	0.08	1.19	0.11	9.2
Ba	684	672	5	659	11	660	19	684	33	4.8
La	25.3	24.4	0.2	24.76	0.42	24.5	0.7	25.2	1.3	5.2
Ce	53.6	51.9	0.3	51.73	0.82	50.5	1.6	53.0	2.4	4.5
Pr	6.83	6.48	0.05	6.83	0.12	6.8	0.3	7.02	0.37	5.3
Nd	28.6	28.4	0.2	28.32	0.51	29.0	1.1	29.8	1.8	6.0
Sm	6.67	6.58	0.08	6.588	0.095	6.6	0.4	6.73	0.45	6.7
Eu	2.00	1.98	0.02	2.040	0.039	1.92	0.12	2.03	0.12	5.9
Tb	1.04	1.06	0.02	1.07	0.02			0.997	0.069	6.9
Gd	6.80	6.67	0.05	6.8	0.1	6.5	0.4	6.5	0.5	7.7
Dy	6.38	6.33	0.07	6.281	0.095	6.5	0.4	6.4	0.5	7.8
Ho	1.29	1.32	0.01	1.307	0.032	1.31	0.08	1.321	0.096	7.3
Er	3.66	3.73	0.04	3.662	0.063	3.6	0.2	3.6	0.3	8.3
Yb	3.34	3.34	0.04	3.282	0.049	3.5	0.2	3.48	0.28	8.0
Lu	0.51	0.50	0.01	0.4894	0.0064	0.51	0.03	0.52	0.04	7.7
Hf	5.17	4.90	0.05	4.756	0.046	5.0	0.3	5.06	0.45	8.9
Ta	0.78	0.81	0.01	0.75	0.044	0.78	0.05	0.82	0.14	17.1
Pb	10.3	10.3	0.2	10.32	0.62	11.5	0.6	11.3	1.3	11.5
Th	5.98	6.03	0.08	6.10	0.11	6.1	0.3	6.24	0.53	8.5
U	1.70	1.62	0.03	1.666	0.029	1.73	0.09	1.93	0.17	8.8

The first columns represent data obtained by solution ICPMS analyses, the last columns data obtained by laser ablation ICP-MS analyses. The data are from the following sources: 'Memorial', unpublished data obtained using a VG PlasmaQuad II at Memorial University, Newfoundland, kindly made available through the courtesy of S. E. Jackson.; 'Norman *et al.*', data published by Norman *et al.* (1996); GEMOC, unpublished data obtained on Agilent 7500s at GEMOC, Macquarie University. RSD, relative standard deviation.

Whole-rock major-element analyses of the xenoliths were performed on fused pellets using 9:1 dilution with sodium tetraborate, and mass absorption corrections, using a Philips PW 2400 X-ray fluorescence (XRF) spectrograph with X47 software at the Institute of Geology, University of Oslo (Table 10).

Whole-rock trace element concentrations were obtained by various methods (Table 10). Data on selected trace elements were obtained by XRF spectrometry on pressed powder pellets (cemented by Paraloid), using matrix corrections based on Compton Top measurements. Many samples were analysed for trace elements by ICPMS at ACTLABS, Ancaster, Ontario, Canada. Finally, some samples were analysed by epithermal instrumental neutron activation analysis (INAA) at the Mineralogical–Geological Museum, University of Oslo, using the method described by Brunfelt & Steinnes (1969). The international rock standards BCR-1, BHVO-1 and G-2 were used for calibration [using standard values recommended by Govindaraju (1989)], and included as unknowns in each run. In general, there is good agreement between results obtained by different methods on the same samples.

For whole-rock Sr and Nd isotope analyses (Table 11), rock powders were leached in cold 0.3M HCl for 2 h, followed by 6M HCl at 80°C for 2 h to remove low-temperature alteration phases. The samples were then rinsed several times in ultrapure water before dissolution. All whole-rock samples were analysed on a Finnegan-MAT 262 mass spectrometer at the Mineralogical–Geological Museum in Oslo. Nd and Sr isotopic compositions are corrected for mass fractionation within run by normalizing to $^{146}\text{Nd}/^{144}\text{Nd} = 0.7219$ and $^{86}\text{Sr}/^{88}\text{Sr} = 0.1194$, respectively. Repeated analyses of the NBS 987 Sr standard gave mean values of $^{87}\text{Sr}/^{86}\text{Sr} = 0.710187 \pm 0.000013$, and the SCS A Nd gave $^{143}\text{Nd}/^{144}\text{Nd} = 0.511116 \pm 0.000008$ during the period when the analyses were made.

Hand-picked clinopyroxene separates (125–250 μm diameter) were washed in ethanol and water and subsequently leached in 6N HCl at 80°C for 4 h, before being rinsed and dissolved. Dissolution was carried out in sealed 15 ml Savillex beakers using a HNO_3 –HF mixture held at 120°C for 48 h. Subsequent chemical procedures, carried out at the University of Oslo, were based on those described by Mearns (1986) and Neumann *et al.* (1990). The samples were analysed for Sr and Nd isotopic compositions using a Finnegan-MAT 262 mass spectrometer at the Vrije Universiteit, Amsterdam, operating in the dynamic mode. Results (Table 11) were normalized to $^{86}\text{Sr}/^{88}\text{Sr} = 0.1194$ and $^{146}\text{Nd}/^{144}\text{Nd} = 0.7219$. NBS 987 (Sr) and La Jolla (Nd) standards measured concurrently gave values for $^{87}\text{Sr}/^{86}\text{Sr}$ and $^{143}\text{Nd}/^{144}\text{Nd}$ of 0.71025 ± 1 and 0.51185 ± 1 , respectively.

All data reported in Table 11 are normalized to the $^{87}\text{Sr}/^{86}\text{Sr}$ standard value of 0.71025.

MINERAL CHEMISTRY

Olivine

Olivine in spinel harzburgites and lherzolites from Tenerife falls within the range $\text{Fo}_{89.0-91.2}$ (Table 2; E.-R. Neumann, unpublished data, 2000). The three groups overlap with respect to incompatible trace elements (Table 2; Fig. 4), although olivine in HEXO is more depleted in Al and Ti than that in HLCO and HTR. Olivine in dunite ($\text{Fo}_{87.2-89.0}$) and wehrlite (about Fo_{90}) is more depleted in middle and light rare earth elements (MREE and LREE, respectively) than that in harzburgites and lherzolites, but falls within their range with respect to heavy rare earth elements (HREE). Olivine in wehrlite TF14-35 shows anomalously high concentrations in Hf (and Zr) (Fig. 4), the reason for which is unclear.

Orthopyroxene

Orthopyroxene in spinel harzburgites and lherzolites is, on average, depleted in Al_2O_3 (≤ 2.3 wt %) and TiO_2 (≤ 0.32 wt %; Table 3) relative to orthopyroxene in peridotites collected along the Mid-Atlantic Ridge and associated fracture zones (1.7–6.1 wt % Al_2O_3 , 0.0–0.2 wt % TiO_2 ; Johnson *et al.*, 1990; Bonatti *et al.*, 1992; Johnson & Dick, 1992). Zoning with increasing TiO_2 and Al_2O_3 from cores to rims of larger grains and neoblasts is common (Fig. 5a).

Orthopyroxene in HEXO shows upwards-concave primordial mantle (PM)-normalized trace element patterns with REE concentrations within the range of orthopyroxene in the strongly depleted harzburgite xenoliths from Lanzarote (Fig. 6a; Table 4), but, in contrast to the latter, they are strongly enriched in the most strongly incompatible elements (e.g. $\text{Rb} = 9 \times \text{PM}$; $\text{Nb} = 4 \times \text{PM}$). It should be noticed, however, that the exsolved orthopyroxene in HEXO is so rich in densely spaced silicate glass inclusions that it is virtually impossible to obtain analyses of pure orthopyroxene. The observed trace element patterns for orthopyroxene in HEXO are therefore interpreted as composite, a combination of depleted orthopyroxene and enriched silicate glass inclusions.

Most poikilitic orthopyroxene in HLCO and HTR is strongly enriched in incompatible trace elements and depleted in Sc, V and Cr relative to that in spinel harzburgites from Lanzarote, and shows negative anomalies in Sr, Zr–Hf and Ti (Fig. 6b), which decrease with increasing REE contents (Fig. 6). Significant variations in trace element concentrations are seen at

Table 2: Average trace element compositions of olivine in spinel harzburgite and lherzolite xenoliths from Tenerife

Island:	Tenerife								Lanzarote	
Rock:	HEXO	HTR			HLCO			Sp dunite	Sp wehr	Sp harz
Sample:	TF14-52	TF14-47	TF14-58	TF14-36	TF14-38	TF14-59	TF14-50	TF14-35		
n:	7	6	6	5	9	7	6	5	24	
mg-no.	91.1		90.6	90.6	90.5		88.9	90.3	89.3-91.6	
Li	4.2	4.4	3.3	3.1	2.6	3.7	2.7	2.4	1.05	
B	3.6	5.5	6.4	1.2	2.5	1.8	1.3	3.7	1.7	
Al	53	104	148	188	126	104	102	113	41	
Ca	370	780	830	680	770	670	1180	900	190	
Sc	3.7	3.7	3.6	3.5	3.6	3.8	5.0	3.0	2.48	
Ti	2.7	81	116	88	39	65	22	74	0.8	
V	3.8	6.1	6.0	6.2	5.4	5.6	4.0	2.8	1.15	
Cr	146	232	198	176	198	212	94	134	21	
Mn	1060	1140	2190	1130	1210	1230	1350	4120	1020	
Co	141	148	132	130	140	150	152	128	146	
Ni	2870	3000	2250	2410	2770	3080	2180	2340	3150	
Cu	13	16	22	18	14	23	12	17	15	
Zn	60	80	170	80	90	90	70	140	60	
Ga	0.16	0.20	0.29	0.29	0.21	0.29	0.16	0.23	0.13	
Rb	<0.044	<0.033	<0.011	0.111	0.069	0.019	0.101	0.153	<0.03	
Sr	0.11	0.05	0.12	0.24	0.15	0.07	0.03	0.02	0.02	
Y	0.28	0.09	0.18	0.15	0.31	0.16	0.26	0.16	<0.01	
Zr	0.12	0.08	0.17	0.17	0.13	0.12	0.06	0.34	<0.01	
Nb	0.070	0.009	0.064	0.175	0.081	0.014	0.006	0.091	<0.005	
Cs	<0.019	<0.014	<0.0068	0.009	<0.019	<0.0055	0.018	0.029	<0.023	
Ba	<0.02	<0.015	0.07	0.09	0.06	0.03	0.21	<0.02	<0.07	
La	0.017	0.005	0.008	0.032	0.017	0.007	0.004	0.003	<0.003	
Ce	0.032	0.013	0.022	0.082	0.036	0.017	0.010	0.006	0.006	
Pr	0.0044	<0.0012	0.0029	0.0063	0.0052	0.0056	<0.0019	0.0033	<0.01	
Nd	<0.015	0.014	<0.006	0.026	0.019	0.014	0.010	<0.009	<0.011	
Sm	<0.011	<0.007	<0.006	<0.007	<0.008	0.003	<0.010	<0.009	<0.01	
Eu	<0.004	<0.003	0.004	<0.002	<0.004	<0.001	<0.005	0.003	<0.004	
Gd	0.012	0.008	0.007	<0.006	0.009	0.006	<0.008	0.007	<0.01	
Tb	<0.005	<0.003	<0.004	<0.004	<0.004	<0.003	<0.005	<0.005	<0.005	
Dy	0.038	0.014	0.018	0.020	0.021	0.014	0.024	0.016	<0.02	
Ho	0.010	0.003	0.006	0.004	0.007	0.005	0.007	0.006	<0.03	
Er	0.037	0.012	0.029	0.019	0.033	0.022	0.036	0.039	<0.01	
Tm	0.009	0.003	0.006	0.004	0.009	0.005	0.007	0.006	<0.003	
Yb	0.08	0.02	0.08	0.04	0.07	0.04	0.06	0.08	<0.02	
Lu	0.015	0.005	0.020	0.008	0.012	0.010	0.011	0.017	<0.003	
Hf	<0.009	<0.004	0.019	<0.006	<0.009	0.005	<0.010	0.257	<0.009	
Ta	<0.003	<0.003	0.004	<0.002	<0.003	<0.001	<0.003	0.007	<0.003	
Th	<0.003	<0.003	0.003	<0.003	<0.004	<0.001	<0.004	<0.003	<0.005	

n, number of analyses; HEXO, harzburgites with exsolved orthopyroxene; HLCO, harzburgites and lherzolites with 'clear', poikilitic orthopyroxene without visible exsolution lamellae; HTR, harzburgites with transitional textures.

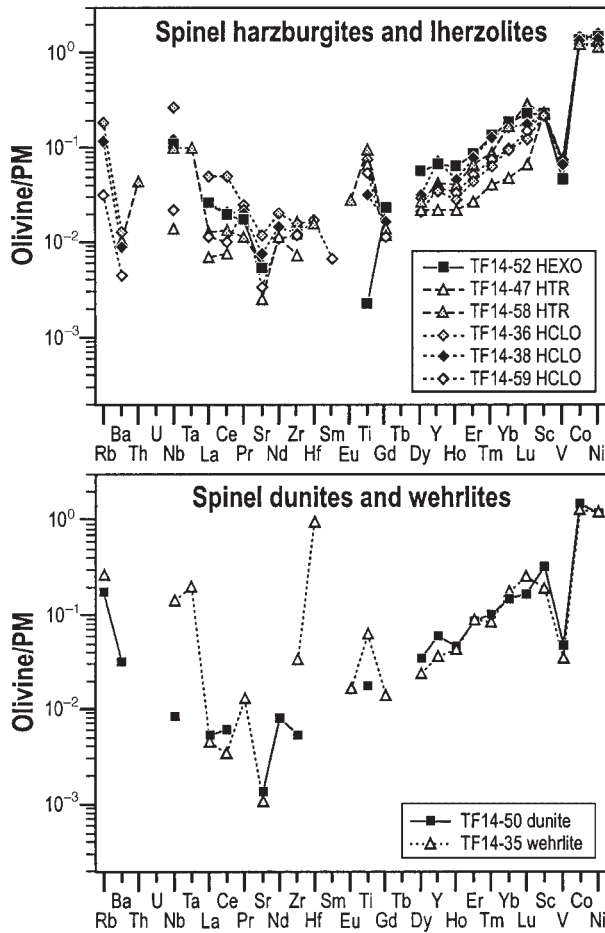


Fig. 4. Average trace element concentrations in olivines in mantle xenoliths from Tenerife, normalized to primordial mantle (PM), using data from McDonough & Sun (1995).

the scale of a thin-section. As the poikilitic orthopyroxene shows no visible fluid inclusions, we believe the observed compositional ranges to represent orthopyroxenes alone. In Table 4 and Fig. 6 separate averages are presented for populations of different compositions (I, II, etc. in Table 4; different signatures in Fig. 6). In addition to enriched orthopyroxene, sample TF14-36 contains grains of strongly depleted orthopyroxene (TF14-36opxII), which fall within the range of orthopyroxene from Lanzarote.

Orthopyroxene in spinel dunites and wehrlites is strongly depleted in Al_2O_3 (<0.8 wt %), but shows a considerable range in TiO_2 (≤ 0.17 wt %; Table 3).

Clinopyroxene

Clinopyroxene in spinel harzburgite and lherzolite xenoliths is Cr-diopside, covering a considerable range in

TiO_2 (0.01–1.7 wt %), Al_2O_3 (0.3–4.2 wt %), Cr_2O_3 (1.0–3.7 wt %), and Na_2O (0.7–2.5 wt %; Table 5). Compositional zoning with increasing Ti and Al, and decreasing Cr and Na, from core to rim is common (Fig. 5b; Table 5).

Like the orthopyroxene, the clinopyroxene shows variations in trace element compositions at the scale of a thin-section. Separate averages, calculated from grains with significantly different compositions within single samples, are presented as I, II, etc. in Table 6 and different signatures in Fig. 7. In all three harzburgite–lherzolite groups the clinopyroxene has relatively high REE contents [Fig. 7; e.g. La (6–300) \times PM], is mildly enriched in LREE relative to HREE, and strongly depleted in Sr, Zr–Hf, and Ti relative to REE. As for orthopyroxene, the degree of depletion in Sr, Zr, Hf and Ti relative to REE decreases with increasing REE.

Clinopyroxene in spinel dunites and wehrlites is somewhat richer in TiO_2 (0.1–1.7 wt %) and Al_2O_3 (0.3–6.7 wt %; Table 5), and tends towards lower MgO , Cr_2O_3 and Na_2O contents than clinopyroxene in the harzburgites and lherzolites, but has similar zoning patterns and PM-normalized trace element patterns (Table 6; Fig. 7c).

Spinel

The spinel in harzburgites and lherzolites from Tenerife is chromite that is generally richer in TiO_2 (0.4–2 wt %) and Cr_2O_3 [cr -number = cation proportion $\text{Cr}/(\text{Cr} + \text{Al}) = 0.5$ –0.9; Table 7] than spinel in peridotites collected along the Mid-Atlantic Ridge and associated fracture zones (≤ 0.7 wt % TiO_2 , cr -number = 0.2–0.6; Bonatti *et al.*, 1992). The highest TiO_2 concentrations and cr -numbers are found in HLCO and HTR. Spinel in wehrlites falls within the compositional range of spinel in harzburgites and lherzolites, whereas most spinel in dunites shows lower cr -number (0.2–0.8) and higher TiO_2 contents (0.5–11.4 wt %; Table 7). The spinel grains are too small to be analysed for trace elements.

Phlogopite

Phlogopite exhibits a wide compositional range, e.g. 0.3–8.5 wt % TiO_2 , 12.2–15.1 wt % Al_2O_3 , 18.7–25.4 wt % MgO , and 0.3–1.3 wt % Na_2O (Table 8). The lowest Al and highest Mg and Na contents are found for sample TF14-42 with ~ 5 vol. % interstitial phlogopite.

Table 3: Representative major element compositions of orthopyroxene porphyroclasts in mantle xenoliths from Tenerife

Rock:	HEXO					HTR					
Sample:	TF14-2		TF14-8			TF14-54		TF14-58			
Grain:	porph		porph		neobl	porph (exs)		porph (clear)		porph (clear)	
	exs core	clear rim	exs core	clear rim	core	core	rim	core	rim	core	rim
wt %											
SiO ₂	57.38	56.06	57.27	58.60	59.24	56.66	56.92	57.77	56.88	57.81	57.48
TiO ₂	0.02	0.28	0.00	0.04	0.00	0.01	0.04	0.08	0.32	0.01	0.24
Al ₂ O ₃	1.26	2.25	0.94	0.63	0.29	1.74	1.11	0.79	1.66	0.55	1.07
Cr ₂ O ₃	0.59	0.61	0.44	0.52	0.15	0.54	0.26	0.32	0.53	0.27	0.42
FeO _{total}	5.65	5.83	5.33	5.36	5.32	6.66	7.11	5.72	5.82	5.74	5.58
MnO	0.15	0.16	0.24	0.22	0.17	0.19	0.22	0.13	0.13	0.17	0.16
MgO	34.00	33.02	34.08	34.57	34.72	33.44	33.64	34.03	33.60	34.15	33.89
NiO	0.08	0.16	0.04	0.01	0.02	0.10	0.08	0.13	0.10	0.08	0.13
CaO	1.15	1.35	0.99	0.99	0.70	0.87	0.99	1.29	1.26	1.32	1.30
Na ₂ O	0.07	0.08	0.08	0.06	0.09	0.06	0.03	0.10	0.06	0.08	0.07
Sum	100.35	99.80	99.41	101.00	100.70	100.27	100.27	100.36	100.36	100.18	100.34
Rock:	HLCO					Spinel dunite				Spinel wehrlite	
Sample:	TF14-3		TF14-36			TF14-4		TF14-46			
Grain:	poikilitic (clear)		bleb in	G1 (clear)		G3 (clear)		inclusion in ol		poikilitic	
	core	rim	cpx	core	rim	core	rim	core	rim	core	rim
wt %											
SiO ₂	58.46	57.22	56.92	58.35	56.88	58.65	57.75	58.07	58.61	58.54	57.93
TiO ₂	0.02	0.20	0.12	0.08	0.27	0.01	0.11	0.16	0.03	0.01	0.06
Al ₂ O ₃	0.31	1.27	1.55	0.32	1.43	0.21	0.50	0.76	0.17	0.41	0.65
Cr ₂ O ₃	0.31	0.48	0.41	0.42	0.53	0.35	0.50	0.22	0.07	0.17	0.22
FeO _{total}	5.52	5.86	6.83	5.39	5.82	5.44	5.37	6.89	6.81	5.67	5.94
MnO	0.15	0.18	0.17	0.13	0.13	0.17	0.18	0.35	0.33	0.48	0.50
MgO	34.69	33.19	32.83	34.26	33.50	34.39	33.87	32.80	33.52	34.35	33.75
NiO	0.09	0.10	0.06	0.07	0.08	0.14	0.13	0.06	0.07	0.10	0.11
CaO	0.76	1.28	1.29	1.43	1.45	1.55	1.48	1.10	0.83	0.89	1.16
Na ₂ O	0.07	0.09	0.06	0.11	0.08	0.14	0.11	0.06	0.08	0.09	0.09
Sum	100.38	99.87	100.24	100.56	100.17	101.05	100.00	100.47	100.52	100.71	100.41

porph, porphyroclasts; exs, exsolved; neobl, neoblast. Analyses of different grains within the same sample are indicated as G1, G2, etc. HEXO, HLCO and HTR are explained in the footnote to Table 2.

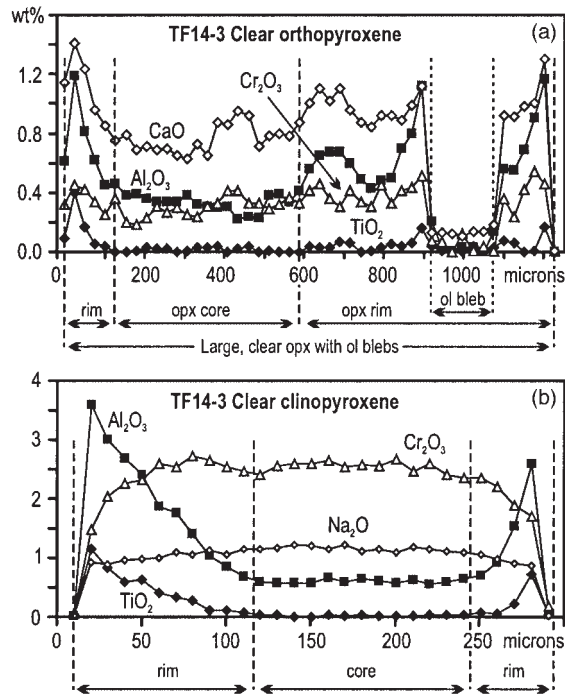


Fig. 5. Profiles through (a) a large, clear, strongly zoned orthopyroxene grain enclosing olivine blebs, and (b) a strongly zoned clinopyroxene in spinel harzburgite TF14-3 (HLCO). It should be noted that the profile through the orthopyroxene (a) passes through an olivine bleb. (See text for further explanation.)

Glass

A general discussion of the major element characteristics of glasses in spinel peridotite xenoliths from different Canary Islands (including Tenerife) was given by Neumann & Wulff-Pedersen (1997). In this paper we present trace element data for glasses in three harzburgites and two lherzolites from Tenerife (Table 9). Glasses in Tenerife xenoliths are silicic (56–63 wt % SiO_2) and alkaline (3.5–5.1% Na_2O , 3.8–4.5% K_2O), and strongly enriched in highly incompatible trace elements [e.g. La: (43–270) \times PM]. PM-normalized trace element patterns show semi-linear REE patterns enriched in LREE relative to HREE, weak negative anomalies for Sr and Ti, and positive ones for Nb (Fig. 8). The strongest enrichment in LREE is found for glasses in lherzolite TF14-39, which also contains the most LREE-enriched clinopyroxene.

WHOLE-ROCK CHEMISTRY

The Tenerife peridotite xenoliths have *mg*-number [cation proportion $Mg \times 100 / (Mg + Fe_{total})$] of 87.9–91.1, but are generally depleted in TiO_2 (<0.2 wt %) and Al_2O_3 (<0.9 wt %; Table 10), show a wide range in CaO

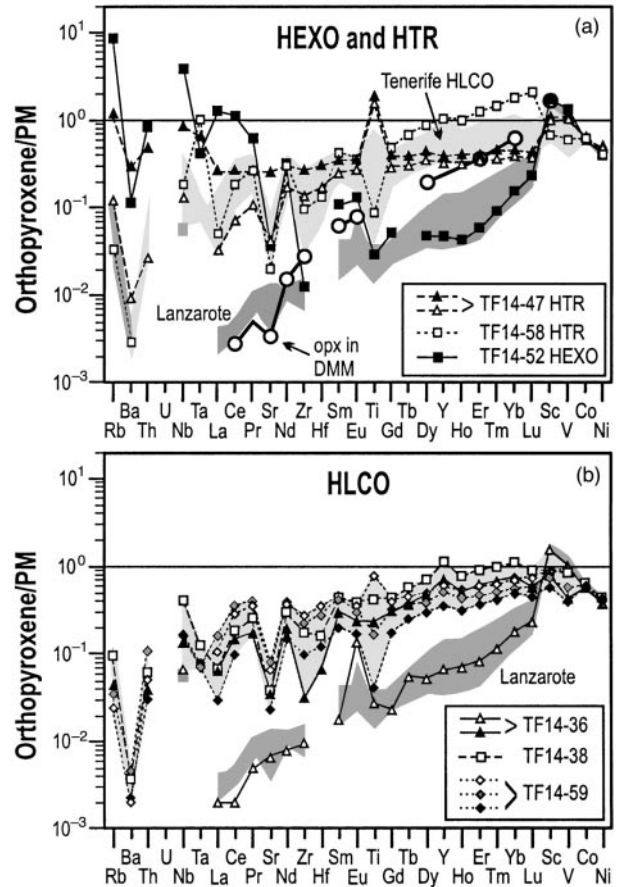


Fig. 6. Average trace element concentrations in orthopyroxenes in (a) HEXO and HTR, and (b) HLCO mantle xenoliths from Tenerife, normalized to primordial mantle (PM), using data from McDonough & Sun (1995). Grains or populations of different compositions within the same sample are presented separately. For comparison are shown the field (dark grey) of orthopyroxene in spinel peridotites in Lanzarote (E.-R. Neumann, unpublished data, 2001), and a hypothetical trace element pattern for orthopyroxene in depleted MORB mantle (DMM), estimated on the basis of cpx–opx distribution coefficients [data from Garrido *et al.* (2000)] and the average composition of clinopyroxene in abyssal harzburgites and lherzolites [data from Johnson *et al.* (1990) and Johnson & Dick (1992)]. The light grey field in (a), showing orthopyroxene in Tenerife HLCO, is taken from (b).

concentrations (0.7–3.0 wt %), and are enriched in strongly incompatible trace elements (e.g. La = (0.4–3) \times PM; Fig. 9) and in LREE relative to HREE. HEXO exhibit pronounced depletion in Sr and Ti relative to REE (Fig. 9). In general, the concentrations in HREE and Sr increase from HEXO through HTR to HLCO, whereas Zr and Hf decrease. The high modal phlogopite content in sample TF14-42 (HLCO) is reflected in high concentrations of Rb, Ba and K (e.g. 0.25 wt % K_2O ; Table 10; Fig. 9). With the exceptions of elements for which data are below the detection limit in major phases

Table 4: Average trace element compositions of orthopyroxene porphyroclasts in mantle xenoliths from Tenerife

Rock:	HEXO	HTR			HLCO					
Sample:	T14-52	TF14-47		TF14-58	TF14-36		TF14-38	TF14-59		
Population:		I	II		I	II		I	II	III
n:	6	4	3	5	5	2	7	4	2	2
Li	1.54	2.20	2.13	1.54	1.61	1.16	1.34	1.64	1.66	1.78
B	13.48	21.94	34.27	7.88	2.82	0.91	6.95	1.56	1.50	1.70
Al	12080	5510	6790	29810	1580	10560	5330	1560	2390	52230
Ca	9000	9310	9710	5420	8340	8520	7910	5990	7400	7820
Sc	27.01	15.66	17.18	10.69	12.84	24.89	14.21	9.29	11.79	14.28
Ti	33	1820	2155	103	278	32	507	48	202	940
V	103	79	88	48	35	85	69	32	47	75
Cr	5710	4210	4360	2700	2840	4530	3190	2360	2860	4240
Mn	1110	1170	1140	2290	1190	1080	1290	1110	1130	1170
Co	59	66	64	64	59	60	65	61	63	64
Ni	764	872	905	789	755	759	840	766	821	848
Cu	8.7	18.4	38.0	17.5	12.7	12.4	11.5	15.1	19.2	24.0
Zn	44	53	50	119	52	47	70	56	58	62
Ga	2.03	2.41	2.68	2.44	1.04	1.83	2.71	1.40	1.95	3.34
Rb	4.954	0.069	0.67	0.020	0.026	<0.011	0.057	<0.014	0.021	0.014
Sr	0.71	0.80	4.93	0.39	0.68	0.13	0.73	0.45	1.54	1.29
Y	0.2	1.4	1.6	4.5	3.0	0.3	4.7	1.5	2.2	2.6
Zr	0.128	1.40	2.75	0.99	0.33	0.10	1.8	1.01	2.36	2.86
Nb	2.43	0.08	0.54	0.12	0.09	0.04	0.27	0.11	0.10	0.11
Cs	0.089	<0.015	0.048	<0.007	<0.008	0.170	<0.015	<0.005	<0.005	<0.005
Ba	0.765	0.059	1.87	0.019	<0.009	<0.010	0.024	0.014	0.029	0.013
La	0.789	0.021	0.166	0.032	0.041	0.001	0.044	0.019	0.102	0.068
Ce	1.81	0.12	0.43	0.31	0.25	<0.01	0.30	0.16	0.59	0.48
Pr	0.151	0.027	0.065	0.068	0.043	0.001	0.063	<0.007	0.101	0.088
Nd	0.38	0.20	0.36	0.38	0.24	0.01	0.36	0.18	0.51	0.46
Sm	0.044	0.103	0.139	0.174	0.120	0.007	0.173	0.080	0.170	0.179
Eu	0.019	0.041	0.053	0.055	0.036	0.021	0.060	0.025	0.045	0.055
Gd	0.03	0.16	0.21	0.26	0.17	0.01	0.23	0.10	0.17	0.22
Tb	<0.003	0.029	0.037	0.069	0.036	0.005	0.056	0.025	0.037	0.044
Dy	0.03	0.23	0.28	0.59	0.31	0.04	0.47	0.20	0.26	0.33
Ho	0.006	0.048	0.058	0.148	0.077	0.011	0.113	0.046	0.065	0.080
Er	0.03	0.15	0.17	0.53	0.27	0.04	0.40	0.16	0.20	0.26
Tm	0.006	0.024	0.030	0.098	0.047	0.008	0.068	0.028	0.035	0.043
Yb	0.07	0.17	0.20	0.78	0.33	0.08	0.49	0.22	0.25	0.32
Lu	0.015	0.025	0.029	0.140	0.039	0.016	0.062	0.031	0.039	0.050
Hf	<0.008	0.048	0.082	0.037	0.019	<0.006	0.045	0.034	0.079	0.101
Ta	0.0152	<0.0029	0.0229	<0.0021	<0.0020	<0.0022	0.0046	0.0027	0.0026	0.0030
Th	0.0650	0.0021	0.0367	<0.0019	0.0031	<0.0023	0.0045	0.0024	0.0085	0.0039

n, number of analyses. Populations of different compositions within the same sample are presented separately as I, II, etc. HEXO, HTR and HLCO are explained in the footnote to Table 2.

Table 5: Representative major element analyses of clinopyroxenes in mantle xenoliths from Tenerife

Rock:	HEXO				HTR		HLCO			
Sample:	TF14-2		TF14-8		TF14-58		TF14-36			
Grain:	interst		G1	G4	G1	G2	G1			G6
	core	rim					core	int	rim	
SiO ₂	54.09	52.60	55.18	54.52	55.21	53.58	53.90	51.19	52.50	52.95
TiO ₂	0.05	0.78	0.03	0.05	0.03	0.74	0.31	1.66	0.83	1.23
Al ₂ O ₃	1.33	3.88	0.86	1.07	0.61	2.31	1.37	4.21	3.03	2.76
Cr ₂ O ₃	2.23	1.56	2.66	1.98	2.79	1.58	1.54	1.17	1.48	1.70
FeO _{total}	2.88	3.12	3.78	2.88	3.64	3.04	2.87	3.25	3.35	3.13
MnO	0.07	0.07	0.11	0.10	0.18	0.14	0.10	0.15	0.08	n.d.
MgO	18.05	16.96	15.89	18.03	17.55	17.37	17.83	16.32	17.08	17.42
NiO	0.10	0.08	0.06	0.11	n.d.	0.06	0.02	0.01	0.02	0.06
CaO	20.21	20.25	19.32	20.31	18.49	20.52	20.65	21.01	20.48	20.73
Na ₂ O	0.85	0.89	2.18	0.85	1.41	0.78	0.88	0.84	0.80	0.74
Sum	99.86	100.19	100.07	99.90	99.91	100.12	99.47	99.81	99.65	100.72

Rock:	HLCO				Spinel dunite			Spinel wehrlite		
Sample:	TF14-38		TF14-39	F14-59	TF14-50			TF14-35		
Grain:	G3	G4			G1	G2	G3	G2	G8	
			core	rim						
SiO ₂	55.28	54.03	55.02	55.35	52.15	52.03	51.28	49.42	54.75	53.13
TiO ₂	0.06	0.36	0.05	0.12	1.26	0.39	0.70	1.22	0.06	0.77
Al ₂ O ₃	0.40	1.95	0.75	0.84	3.80	3.28	5.34	6.60	0.29	2.47
Cr ₂ O ₃	2.05	1.60	3.90	1.59	1.24	1.14	1.07	0.84	3.88	1.94
FeO _{total}	4.36	3.28	3.35	2.98	3.14	3.10	3.62	3.81	2.48	2.97
MnO	0.08	0.15	0.11	0.10	0.07	0.11	0.09	0.06	0.25	0.33
MgO	17.58	17.58	15.33	19.31	16.55	15.71	15.38	14.44	16.92	16.98
NiO	0.11	0.02	0.02	0.01	n.d.	0.04	0.10	n.d.	0.05	n.d.
CaO	19.91	20.52	18.87	19.61	21.32	23.65	21.87	22.40	18.97	20.77
Na ₂ O	1.17	0.77	2.53	0.74	0.82	0.57	0.76	0.77	1.48	0.81
Sum	101.00	100.34	99.93	100.65	100.35	100.02	100.21	99.56	99.13	100.17

n.d., not detected. Different grains are identified as G1, G2, etc.

(e.g. Rb, Ba, Ta), there is reasonably good agreement between measured whole-rock compositions and whole-rock compositions estimated on the basis of mineral and glass analyses and modal relationships (not shown).

Also, the dunites and wehrlites are highly refractory with respect to TiO₂ and Al₂O₃ (dunites: 0.06 wt % TiO₂, 0.6–0.7 wt % Al₂O₃; wehrlites: 0.15–0.17 wt % TiO₂, 0.6–0.9 wt % Al₂O₃; Table 10). PM-normalized trace element patterns resemble those of harzburgites

Table 6: Average trace element compositions of clinopyroxenes in mantle xenoliths from Tenerife

Rock:	HEXO	HTR				HLCO				
Sample:	TF14-52	TF14-58		TF14-47		TF14-36			TF14-38	
Population:		I	II	I	II	I	II	III	I	II
n:	3	2	6	4	3	2	3	3	3	4
Li	1.03	1.23	1.46	1.49	1.48	1.23	1.24	1.52	1.02	1.19
Be	0.55	0.11	0.22	0.10	0.14	1.05	3.90	0.72	2.57	3.54
B	9.2	1.4	1.6	2.1	1.5	3.8	6.9	11.2	3.9	8.9
Al	7780	2970	6720	15250	22030	13260	12470	2960	2170	10960
P	27	18	41	55	53	57	33	28	15	30
Sc	166	166	81	80	53	77	82	95	113	81
Ti	50	110	3600	5370	9760	3700	1760	736	207	1520
V	351	308	241	265	311	287	255	181	84	273
Co	23.7	19.5	23.1	23.7	21.5	22.0	22.2	24.1	17.8	23.0
Ni	375	339	357	308	273	339	377	363	258	363
Ga	2.9	1.4	2.6	6.5	8.4	3.4	4.0	1.6	1.3	3.9
Rb	0.21	<0.04	<0.06	0.66	n.d.	0.33	0.1	<0.05	2.4	0.3
Sr	31.9	47.0	129	146	110	148	183	138	102	190
Y	57	8	14	77	35	58	70	46	45	67
Zr	20	n.d.	16	67	56	30	15	8	6	30
Nb	3.62	0.21	0.26	0.73	0.47	1.29	1.28	0.63	3.81	2.15
Cs	<0.02	<0.02	<0.03	0.03	<0.02	<0.02	<0.01	<0.02	0.12	<0.02
Ba	0.10	0.03	0.04	0.77	0.27	0.47	0.45	0.57	1.08	0.24
La	83	6	4	16	5	12	17	14	11	16
Ce	227	14	16	67	20	46	64	52	40	67
Pr	25	2	3	11	4	7	10	8	6	11
Nd	74	7	16	51	23	34	41	33	25	45
Sm	13	2	5	13	7	9	11	8	6	11
Eu	3.0	0.5	1.5	3.5	2.1	2.3	2.6	1.9	1.7	3.0
Gd	9.0	1.3	4.5	12.4	7.4	8.2	8.9	6.4	5.4	9.4
Tb	1.6	0.2	0.6	2.2	1.2	1.3	1.4	1.0	0.9	1.6
Dy	11	1	3	15	7	8	9	7	6	10
Ho	2.1	0.2	0.6	3.0	1.5	1.5	1.7	1.2	1.2	1.9
Er	5.8	0.6	1.3	8.2	3.9	4.0	4.4	3.2	3.2	4.9
Tm	0.82	0.08	0.15	1.24	0.56	0.52	0.57	0.43	0.44	0.66
Yb	5.0	0.5	0.8	8.4	3.8	3.0	3.1	2.3	2.4	3.7
Lu	0.60	0.07	0.11	1.17	0.57	0.29	0.31	0.24	0.26	0.39
Hf	0.3	n.d.	0.6	3.6	2.9	0.9	0.4	0.2	0.1	1.1
Ta	0.14	0.002	0.008	0.094	0.086	0.061	0.037	0.066	0.073	0.078
Pb	1.2	0.5	0.1	0.2	0.1	0.2	0.4	0.4	0.2	0.3
Th	0.32	0.01	0.01	0.05	0.04	0.07	0.07	0.02	0.13	0.10
U	0.048	<0.002	0.003	0.012	0.009	0.017	0.007	0.005	0.018	0.022

Rock:	HLCO			Spinel dunite		Spinel wehrlite		
Sample:	TF14-39	TF14-59		TF14-50		TF14-35		
Population:		I	II	I	II	I	II	III
<i>n</i> :	7	3	3	3	3	2	4	2
Li	0.93	1.19	1.23	0.76	0.76	1.32	1.94	2.02
Be	0.58	0.55	0.19	0.95	0.68	0.80	0.55	0.48
B	5.0	1.2	6.7	1.1	1.8	2.0	1.7	0.8
Al	4260	15800	3840	28300	23200	25500	6460	2550
P	32	65	19	25	30	56	50	28
Sc	112	82	89	107	124	57	76	113
Ti	235	5860	314	3610	1830	5860	1840	511
V	280	300	165	320	240	150	120	98
Co	17.0	21.2	25.8	22.0	20.5	21.7	36.2	23.4
Ni	253	331	395	284	312	327	589	358
Ga	4.0	5.4	2.0	5.2	4.2	5.0	3.0	1.5
Rb	0.46	0.4	0.4	<0.04	0.25	0.08	0.13	<0.07
Sr	108	122	84	120	34	152	160	120
Y	126	52	32	80	35	27	26	21
Zr	70	91	30	13	5	44	19	9
Nb	2.17	1.25	0.43	0.70	0.50	0.65	0.39	0.37
Cs	<0.02	<0.02	<0.02	<0.02	<0.02	<0.03	<0.04	<0.03
Ba	0.75	0.41	0.94	0.23	1.03	0.09	0.21	0.10
La	178	15	22	31	15	8	7	10
Ce	470	69	85	110	47	26	27	28
Pr	60	12	12	17	7	5	5	5
Nd	191	55	48	73	29	24	23	20
Sm	30	13	9	17	7	7	6	5
Eu	6.3	3.2	2.1	4.0	1.7	2.0	1.7	1.3
Gd	20.5	11.1	6.6	14.9	5.8	6.2	5.4	4.0
Tb	3.3	1.7	1.0	2.3	0.9	0.9	0.8	0.6
Dy	21	10	6	15	6	5	5	4
Ho	4.1	1.9	1.1	2.8	1.2	1.0	0.9	0.7
Er	11.1	4.7	2.9	7.0	3.1	2.5	2.4	1.8
Tm	1.61	0.59	0.36	0.86	0.39	0.34	0.33	0.27
Yb	10.2	3.3	2.0	4.6	2.2	2.2	2.3	1.9
Lu	1.31	0.41	0.25	0.46	0.25	0.34	0.36	0.33
Hf	2.3	3.8	1.0	0.5	0.2	1.7	0.7	0.3
Ta	0.037	0.161	0.016	0.026	0.011	0.066	0.014	0.008
Pb	0.4	0.1	0.3	0.3	0.2	0.1	0.2	0.2
Th	0.13	0.12	0.10	0.40	0.20	0.04	0.02	0.01
U	0.014	0.015	0.007	0.015	0.014	0.009	<0.006	<0.004

n, number of analyses. Populations of different compositions within the same sample are presented separately as I, II, etc. HEXO, HTR and HLCO are explained in the footnote to Table 2.

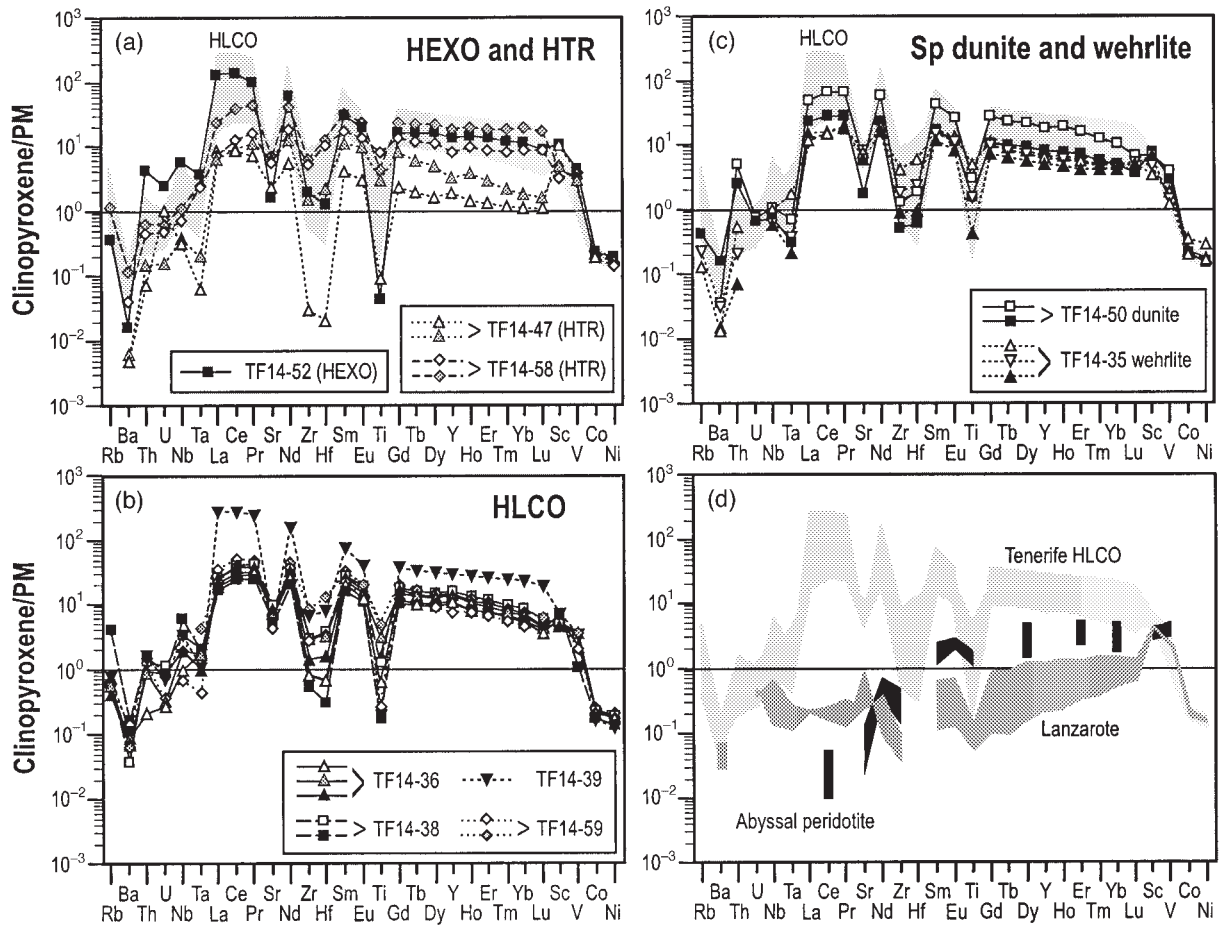


Fig. 7. Average trace element concentrations in clinopyroxenes in different types of mantle xenoliths from Tenerife (a–c), normalized to primordial mantle (PM), using data from McDonough & Sun (1995). Grains or populations of different compositions within the same sample are presented separately. (d) Clinopyroxenes in HLCO compared with clinopyroxenes in ‘normal’ (non-hotspot) abyssal harzburgites and lherzolites [data from Johnson *et al.* (1990) and Johnson & Dick (1992)], and in spinel harzburgites from Lanzarote (E.-R. Neumann, unpublished data, 2001).

and lherzolites (Fig. 9). The wehrlite TF14-35 is highly enriched in Sm and Eu relative to other RE; the reason for this is not clear.

Sr–Nd ISOTOPIC RATIOS

Whole-rock samples and clinopyroxene separates have similar ⁸⁷Sr/⁸⁶Sr and ¹⁴³Nd/¹⁴⁴Nd isotopic ratios (whole rocks 0.70312–0.70334 and 0.51288–0.51295, respectively; clinopyroxene separates 0.70314 and 0.51290–0.51291, respectively; Table 11, Fig. 10). These values partly overlap with, and partly fall to the high ⁸⁷Sr/⁸⁶Sr side of the field occupied by Tenerife basalts (Simonsen *et al.*, 2000). Two clinopyroxenites, believed to have formed at high pressures from mafic

Canarian magmas, give similar ⁸⁷Sr/⁸⁶Sr and ¹⁴³Nd/¹⁴⁴Nd ratios to those for the harzburgites and wehrlites (0.70312–0.70314 and 0.51287–0.51292, respectively, Table 11).

DISCUSSION

Partial melting and depletion

The data presented above imply that the upper mantle beneath Tenerife has been subjected to strong depletion, later overprinted by metasomatism. On the basis of the geophysical and geochemical evidence that all the Canary Islands are built on oceanic lithosphere (Verhoef *et al.*, 1991; Roest *et al.*, 1992; Hoernle, 1998; Neumann *et al.*,

Table 7: Representative major element analyses of spinel in mantle xenoliths from Tenerife

Rock:	HEXO				HTR					
Sample:	TF14-2		TF14-14		TF14-36		TF14-42			
	verm	euhydr	interst	verm	large	large	large	med	med	
	core		rim		core	rim				
SiO ₂	0.06	0.26	0.12	0.21	n.d.	n.d.	n.d.	n.d.	n.d.	
TiO ₂	1.40	0.08	0.86	1.07	0.13	0.35	2.51	0.60	1.67	
Al ₂ O ₃	26.30	14.68	17.64	22.58	14.24	18.88	18.12	7.04	9.91	
Cr ₂ O ₃	38.80	50.29	46.72	41.82	51.72	45.90	45.99	59.66	55.97	
Fe ₂ O ₃	4.91	6.52	5.49	4.76	6.15	7.94	4.55	5.79	4.29	
FeO	12.16	11.71	12.16	12.21	14.76	13.63	14.33	14.80	15.02	
MnO	0.17	0.16	0.17	0.20	0.30	0.29	0.19	0.22	0.20	
MgO	16.34	14.41	14.70	15.51	12.41	13.93	14.77	12.08	12.88	
NiO	0.19	0.24	0.23	0.19	0.30	0.21	0.21	0.06	0.19	
Sum	100.41	98.36	98.14	98.55	100.02	101.33	100.69	100.43	100.14	
Rock:	HLCO									
Sample:	TF14-5		TF14-14		TF14-36		TF14-42			
	large neobl		interst	verm	large	large				
	core		rim							
SiO ₂	0.01	0.06	0.04	0.05	0.01	0.07				
TiO ₂	0.54	0.66	0.38	0.03	1.91	1.64				
Al ₂ O ₃	13.03	14.69	15.73	3.33	15.30	7.72				
Cr ₂ O ₃	54.84	51.42	51.46	62.09	48.87	57.71				
Fe ₂ O ₃	4.54	5.36	5.20	7.13	5.45	4.94				
FeO	14.82	14.45	12.95	17.61	14.42	13.06				
MnO	0.17	0.18	0.28	0.32	0.21	0.75				
MgO	12.89	13.21	14.07	9.37	13.98	13.49				
NiO	0.15	0.12	0.18	0.11	0.22	0.20				
Sum	101.00	100.24	100.32	100.30	100.40	99.57				
Rock:	Spinel dunite				Spinel wehrlite					
Sample:	TF14-4			TF14-35		TF14-46				
	incl cpx	incl cpx	incl	medium		large		medium		
	core		rim	core	rim	core	rim	core		
SiO ₂	0.2	0.06	0.04	0.05	0.01	0.02	0.02	0.02		
TiO ₂	2.85	2.33	2.83	2.71	2.45	0.57	1.27	2.27		
Al ₂ O ₃	13.29	8.27	29.07	19.54	25.69	19.32	11.07	8.59		
Cr ₂ O ₃	46.70	50.45	25.32	42.68	35.59	41.01	51.88	55.85		
Fe ₂ O ₃	7.18	8.76	10.70	5.82	6.24	9.89	6.75	4.21		
FeO	16.43	18.51	15.30	13.93	12.67	15.04	14.93	16.14		
MnO	0.37	0.34	0.27	0.62	0.52	0.57	0.59	0.67		
MgO	12.76	10.59	14.86	14.98	16.14	12.75	12.26	12.03		
NiO	0.15	0.17	0.22	0.28	0.20	0.15	0.22	0.18		
Sum	99.87	99.53	98.75	100.63	99.52	99.34	99.07	99.99		

Fe₂O₃ and FeO are estimated from the structural formulae, assuming full stoichiometry and charge balance. n.d., not detected; verm, vermicular; neobl, neoblasts. The three harzburgite and lherzolite groups (HEXO, HTR, HLCO) are explained in the footnote to Table 2.

Table 8: Representative major element analyses of phlogopite in mantle xenoliths from Tenerife

Rock:	HEXO	HLCO					Wehrlite	
Sample:	TF14-8 incl opx	TF14-14 incl opx	TF14-36 incl ol	TF14-39 incl ol	TF14-42 interst	TF14-42 interst	TF14-35 incl cpx	TF14-46 incl ol
SiO ₂	41.26	41.90	38.08	40.65	41.90	40.94	38.29	41.14
TiO ₂	0.25	0.09	8.54	1.32	0.80	3.07	8.03	0.39
Al ₂ O ₃	13.34	14.14	15.14	13.70	12.25	12.45	15.04	15.12
Cr ₂ O ₃	2.32	1.71	2.22	1.68	0.94	1.30	1.89	1.05
FeO _{total}	3.26	2.93	4.16	3.10	2.01	2.73	4.29	4.34
MnO	n.d.	0.05	n.d.	0.04	0.01	0.08	0.11	0.12
MgO	24.16	24.87	18.67	22.59	25.44	23.67	19.00	23.57
NiO	0.13	0.11	0.29	0.10	0.10	0.11	0.22	0.29
CaO	n.d.	0.04	0.05	0.01	0.01	0.01	0.02	0.04
Na ₂ O	0.34	0.52	0.68	0.68	1.29	1.30	0.73	0.33
K ₂ O	9.76	9.43	9.30	9.56	8.57	8.47	9.16	9.97
Sum	94.82	95.79	97.13	93.43	93.32	94.13	96.78	96.36

n.d.: not detected. HEXO and HLCO are explained in the footnote to Table 2. Incl ol, incl opx, incl cpx, inclusion in olivine, orthopyroxene, clinopyroxene, respectively; interst, interstitial.

2000), we use data on average depleted MORB mantle (DMM) and depleted spinel harzburgites from Lanzarote as a basis for evaluation of the types and extent of chemical changes that have taken place in the upper mantle beneath Tenerife.

The HEXO xenoliths fall close to the oceanic CaO–Al₂O₃ and $mg_{\text{rock}}\text{--Mg/Si}$ trends of Boyd (1996), but are more depleted in CaO and Al₂O₃ than average DMM (Fig. 11). Their concentration range in HREE is only about $(0.2\text{--}0.5) \times \text{PM}$ (Fig. 9). HEXO and one HLCO xenolith (TF14-36) contain highly depleted orthopyroxene similar to that found in Lanzarote xenoliths (Table 4; Fig. 6). As indicated above, the high concentrations in strongly incompatible elements found for orthopyroxene in HEXO are believed to reflect silicate glass inclusions highly enriched in strongly incompatible elements. Also, HLCO and HTR xenoliths exhibit very low Al₂O₃ contents, similar to those in HEXO (Fig. 11). These features imply that all the peridotite xenoliths from Tenerife, like those from Lanzarote, have been subjected to more extensive partial melting and depletion than average DMM.

Evidence of metasomatism in harzburgites and lherzolites

Metasomatic processes are reflected in petrographic observations indicating formation of clinopyroxene and

olivine at the expense of orthopyroxene in HLCO and HTR (Fig. 3c and d), in the presence of phlogopite, and in enrichment in strongly incompatible trace elements (including LREE and MREE) in rocks and minerals relative to DMM and its constituent minerals (Figs 4, 6, 7 and 9). Linear rows of minute spinel inclusions in olivine neoblasts and olivine blebs in orthopyroxene have been interpreted as the remains of spinel exsolution lamellae inherited from decomposed orthopyroxene (Neumann, 1991; Wulff-Pedersen *et al.*, 1996).

Formation of clinopyroxene and olivine at the expense of orthopyroxene is supported by their higher abundance in HLCO than in HEXO (Fig. 2). Progressive partial melting of peridotite at mantle pressures changes the phase assemblage of the residual rock from $ol + opx + cpx \pm sp$ through $ol + opx \pm sp$ to ol (dashed arrows in Fig. 2); clinopyroxene is expected to be exhausted when the residual rock contains 60–80% modal olivine (depending on initial rock composition and pressure; e.g. Jaques & Green, 1980). Mantle xenoliths from Lanzarote contain ($\geq 57\%$ modal olivine; most xenoliths with $>70\%$ olivine have ($\leq 1\%$ clinopyroxene, and many samples lack clinopyroxene altogether (Neumann *et al.*, 1995). Thus, most Lanzarote xenoliths fall on, or close to, the $ol + opx \pm sp$ part of a progressive melting trend. The small amounts of clinopyroxene found in samples with $>70\%$ olivine are probably exsolved from orthopyroxene upon cooling. In contrast, all mantle xenoliths

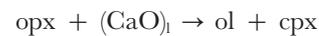
Table 9: Representative major and trace element analyses of glass inclusions and interstitial glasses in spinel harzburgite and lherzolite HLCO xenoliths from Tenerife

Sample:	TF14-36	TF14-36	TF14-36	TF14-36	TF14-38	TF14-38	TF14-39	TF14-39	TF14-39	TF14-59	TF14-59
SiO ₂	56.05	56.01	57.55	56.13	62.22	61.35		63.49	62.67	58.88	58.71
TiO ₂	2.45	2.75	2.85	2.71	0.86	0.79		0.71	1.02	2.45	2.07
Al ₂ O ₃	16.08	16.10	16.76	16.06	16.74	16.46		15.07	15.13	16.11	16.51
Cr ₂ O ₃	n.d.	0.07	0.06	n.d.	0.01	n.d.		0.02	0.02	0.03	0.05
FeO _{total}	3.37	3.38	3.69	3.55	2.73	2.60		2.39	2.49	3.64	2.57
MnO	0.04	0.07	0.05	0.08	0.09	0.05		n.d.	0.02	0.08	0.08
MgO	2.98	3.39	3.33	3.40	2.67	2.22		2.14	2.19	3.30	2.88
NiO	0.04	n.d.	0.02	n.d.	n.d.	0.06		0.04	n.d.	n.d.	0.13
CaO	6.56	7.08	5.01	7.19	4.34	5.09		3.62	3.77	6.29	6.19
Na ₂ O	3.99	4.39	4.28	3.78	4.75	4.55		5.09	5.11	3.51	3.84
K ₂ O	3.91	3.84	4.22	3.91	4.53	4.11		4.46	4.47	3.87	4.19
Sum	95.47	97.08	97.82	96.81	98.94	97.28		97.03	96.89	98.16	97.22
Sc	23.7	20.6	15.2	22.8	9.8	14.1	13.0	18.1	17.8	15.8	23.3
Ti	17450	17970	12040	17690	2790	4320	12770	4140	5810	17430	13090
V	199	190	132	205	103	103	195	174	277	222	146
Ni	540	240	630	1610	2260	220	200	1222	3170	920	800
Sr	832	854	575	769	357	534	469	599	592	764	682
Y	52	36	25	40	21	33	17	57	50	31	48
Zr	360	310	204	317	190	272	224	456	402	309	616
Hf	7.7	6.1	4.5	7.4	3.2	5.4	5.0	10.6	7.1	7.7	13.9
Nb	277	191	121	191	285	427	43	573	426	59	174
Th	16.8	11.5	7.1	11.8	7.7	12.0	2.7	14.7	10.1	3.9	15.0
U	1.82	1.53	1.11	1.52	1.04	1.40	1.50	2.95	2.33	1.17	2.75
La	76.9	64.5	39.7	59.5	41.5	65.1	26.7	185	165	29.8	97.9
Ce	142	122	76	117	79	123	58	345	308	64	203
Pr	16.8	14.2	9.12	14.3	8.40	12.7	8.26	39.0	34.7	8.83	26.5
Nd	62.5	55.1	34.9	54.2	26.6	42.8	32.0	118	106	36.5	94.1
Sm	12.3	10.4	6.80	10.5	4.40	7.53	6.38	15.6	14.0	6.54	14.0
Eu	2.64	2.55	1.60	3.51	1.14	1.87	1.94	2.65	3.10	1.95	3.91
Gd	8.95	7.76	4.69	7.15	3.06	5.21	4.72	10.0	8.35	5.93	10.6
Tb	1.24	1.46	0.72	1.44	0.43	0.97	0.91	1.41	1.17	0.89	1.58
Dy	7.55	6.29	3.70	7.78	2.53	4.54	4.91	9.55	8.00	5.46	8.70
Ho	1.51	1.24	0.90	1.51	0.56	0.90	0.71	1.66	1.47	0.95	1.40
Er	4.73	3.99	2.04	3.75	1.34	2.71	1.90	4.81	4.13	2.87	4.28
Tm	0.58	0.62	0.35	0.60	0.27	0.49	0.15	0.44	0.40	0.57	0.68
Yb	3.27	1.64	2.04	2.98	1.24	1.69	1.39	4.85	5.35	3.58	3.08
Lu	0.46	0.44	0.27	0.45	0.16	0.24	0.29	0.66	0.69	0.51	0.52

n.d., not detected. Major elements in wt %, trace elements in ppm.

from Tenerife contain >73% olivine and significant amounts of clinopyroxene, the highest contents are found in samples with >80% modal olivine. The modal proportions of clinopyroxene in these rocks thus appear to be independent of olivine contents (Fig. 2), strongly suggesting that the clinopyroxene is not part of residual

assemblages, but has formed through metasomatic reactions. The reaction



satisfies both textural and compositional relationships. Finally, HLCO show high whole-rock CaO/Al₂O₃

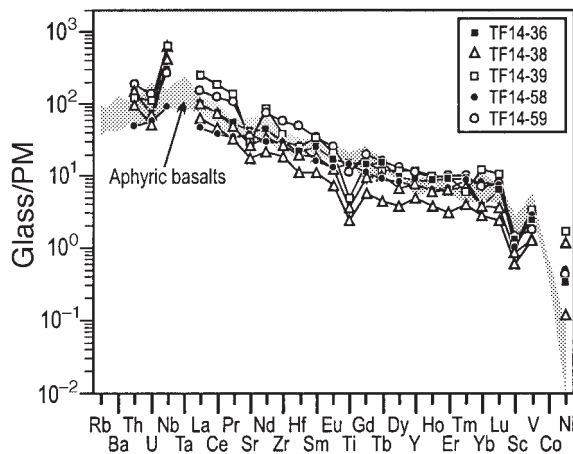


Fig. 8. Trace element concentrations in glasses in spinel harzburgite and lherzolite xenoliths from Tenerife, normalized to primordial mantle (PM), using data from McDonough & Sun (1995). Data on aphyric basalts from Tenerife (Neumann *et al.*, 1999) are shown for comparison.

($\gg 1.0$) relative to DMM (~ 1.0 ; Fig. 11), which was attributed by Boyd (1996) to Ca metasomatism. Moderate Ca metasomatism is also exhibited by HTR, but not by HEXO.

Our results show that in Tenerife Ca metasomatism, as defined by Boyd (1996), is only one reflection of a metasomatic event involving a combination of cryptic and modal metasomatism, addition of iron (causing the rocks to fall below the oceanic Mg/Si-*mg*-number trend; Fig. 11b), and peridotite–fluid or peridotite–melt reactions leading to the formation of Ti–Al–Zr–Hf-depleted and Na–Cr–REE-enriched clinopyroxene. The compositions of the metasomatic transport agent(s) and the nature of the metasomatic processes that have been in operation in the upper mantle beneath Tenerife are discussed below.

Evidence for open-system metasomatism

The Tenerife xenoliths show no simple correlation between the degree of Ca metasomatism and the concentrations of incompatible trace elements (Fig. 12). The metasomatism must consequently involve open-system processes rather than simple two-component mixing. Open-system processes discussed in the literature include (1) the chromatographic effects of melt percolation in the upper mantle (e.g. Navon & Stolper, 1987), (2) infiltration by fluids released from crystallizing silicate melts (Andersen *et al.*, 1984; O'Reilly & Griffin, 1988), and (3) trapping of trace elements in metasomatically introduced acceptor minerals (O'Reilly *et al.*, 1991; Neumann *et al.*, 2000). The last model implies that a metasomatic agent enters a given mass

of mantle rock and causes reactions and chemical exchange between fluid and wall-rock, leaving a residual fluid that moves out of the mantle rock mass in question. The elements most compatible with minerals formed through metasomatic reactions (and with wall-rock minerals) are preferentially partitioned into, and 'trapped' by, these, whereas elements incompatible with all the phases in the metasomatized rock are partitioned into the residual fluid, and transported away.

Textural features indicate that clinopyroxene and phlogopite are formed as the result of metasomatic processes. Furthermore, the clinopyroxene-rich HLCO xenoliths are enriched in Rb, Ba, MREE and HREE relative to HEXO, have similar or slightly higher concentrations in Nb, Ta, Zr and Hf, and are depleted in Th and U (Fig. 13). The La/Yb ratio decreases from HEXO [$(\text{La}/\text{Yb})_N \sim 22$], through HTR [$(\text{La}/\text{Yb})_N \sim 7$], to HLCO [$(\text{La}/\text{Yb})_N \sim 5$]. These features are compatible with trapping of elements by newly formed clinopyroxene and phlogopite [model (3)]. The clinopyroxene structure allows extensive substitution in the M1 and M2 lattice positions by divalent and trivalent trace elements with ionic radii close to the optimal size of these sites, whereas substitution of trace elements with very large ionic radii and/or high valencies is very limited, although substitution of Na for Ca may also be extensive (e.g. Jensen, 1973; Brenan & Watson, 1991; LaTourrette & Burnett, 1992; Klemme *et al.*, 1995; Sweeney *et al.*, 1995; Wood & Blundy, 1997; Blundy *et al.*, 1998). Selective trapping of trace elements by clinopyroxene may explain enrichment in MREE and HREE relative to LREE (causing decreased La/Yb ratios) and other incompatible trace elements in HLCO, as compared with HEXO. Rb, Ba and K are typically trapped by phlogopite (e.g. Nash & Crecraft, 1985; Sweeney *et al.*, 1995; Foley *et al.*, 1996). In view of the insignificant amounts of phlogopite observed in these rocks, trapping in phlogopite should be unimportant. However, the high K_2O contents of silicate glasses in mantle xenoliths from Tenerife (Table 9) suggest that the xenoliths may have contained significant amounts of a K-rich phase (phlogopite) that have been partially or totally consumed by partial melting as part of the metasomatic processes (Neumann & Wulff-Pedersen, 1997). We conclude that the geochemical characteristics of HLCO and HTR are the results of a combination of mixing between a metasomatic fluid and mantle wall-rock, and selective trapping of elements in phases (mainly clinopyroxene, phlogopite) formed as the result of the metasomatic reactions. HEXO have suffered a relatively low degree of metasomatism compared with HLCO.

Metasomatic agents

The data presented above indicate metasomatism by fluid(s) or melt(s) strongly enriched in highly incompatible

Table 10: Bulk-rock analyses of mantle xenoliths from Tenerife

Rock:	HEXO			HTR					HLCO	
Sample:	TF14-40	TF14-52	TF14-53	TF14-45	TF14-47	TF14-57	TF14-58	TF14-61	TF14-36	TF14-38
<i>XRF (wt %)</i>										
SiO ₂	43.00	43.23	43.72	41.89	42.34	43.72	42.82	42.93	41.86	42.83
TiO ₂	0.02	0.02	0.01	0.12	0.11	0.10	0.10	0.12	0.17	0.05
Al ₂ O ₃	0.55	0.64	0.63	0.65	0.43	0.58	0.55	0.79	0.74	0.67
FeO _{total}	8.26	7.89	7.96	7.98	8.34	8.20	8.09	8.39	8.61	8.32
MnO	0.14	0.13	0.13	0.14	0.13	0.14	0.14	0.41	0.15	0.14
MgO	45.68	45.47	44.78	45.80	46.23	44.54	44.65	43.82	43.89	45.40
CaO	0.89	0.73	0.80	0.98	0.82	0.91	1.41	1.27	2.28	0.98
Na ₂ O	0.15	0.11	0.16	0.21	0.09	0.09	0.08	0.13	0.19	0.20
K ₂ O	0.07	0.05	0.10	0.14	0.04	0.03	0.02	0.08	0.07	0.08
P ₂ O ₅	0.01	0.05	0.01	0.03	0.01	0.01	0.01	0.01	0.04	0.01
LOI	-0.36	-0.41	-0.16	-0.37	-0.45	-0.42	0.07	-0.18	-0.11	-0.31
Sum	98.40	97.90	99.01	98.44	99.03	98.82	97.93	97.76	98.42	98.36
<i>XRF (ppm)</i>										
V	46	36					47	32	55	44
Cr	2670	3060					3480	3530	2670	2300
Co	119	115					113	114	116	114
Ni	2510	2420					2410	2410	2320	2480
Zn	51	52					59	197	59	56
Rb	7	5					5	7	6	7
Sr	15	n.d.					19	21	33	26
Y	n.d.	n.d.					n.d.	n.d.	2	n.d.
Zr	20	20					18	19	19	17
Nb	10	9					2	3	5	11
<i>INAA (ppm)</i>										
K	736	500.6					153	789	520	643
Na	1971	1703					1434	1790	2060	2100
Sc	8.94	9.21					8.15	7.88	10.6	8.06
Ga	1.28	0.32					1.9	2.32	1.39	1.19
As	0.66	0.45					0.59	0.53	0.76	0.96
Cs	0.07	0.03					0.02	0.05	0.01	0.22
Ba	3.3	5.9					5.3	12.1	10.7	9.1
La	5.59	3.46					1.24	1.36	2.25	2.22
Ce	7.71	5.42					1.67	2.53	3.1	4.35
Nd	2.86	n.d.					3.22	6.66	8.81	3.86
Sm	0.55	0.41					0.45	0.53	0.9	0.41

elements relative to PM, but less enriched in Ba, K, Sr, P and Ti than in other incompatible trace elements (Fig. 12). In addition, the fluids or melts carried K and H₂O (forming phlogopite), and Fe (Fig. 11). The combination of low Ti–Al and high Na–Cr contents in clinopyroxene cores in HLCO (Table 5) strongly suggests formation

from a very Ti–Al-poor but Na-rich fluid. The common presence of CO₂ inclusions, and association of CO₂ and silicate glass, observed both in polyphase inclusions and in many CO₂-dominated inclusions, imply that the metasomatizing fluids also carried Si and C, although it is unclear if they were primarily silicic or carbonaceous.

Table 10: continued

Sample:	TF14-40	TF14-52	TF14-53	TF14-45	TF14-47	TF14-57	TF14-58	TF14-61	TF14-36	TF14-38
Eu	0.15	0.2					0.12	0.15	0.7	0.3
Gd	1.64	0.29					1.78	0.36	0.91	0.19
Tb	0.06	0.03					0.07	0.08	0.08	0.08
Ho	0.06	0.06					0.09	0.15	0.21	0.13
Yb	0.22	0.31					0.2	0.44	0.43	0.33
Hf	0.18	0.11					0.13	0.23	0.3	0.11
Ta	0.25	0.34					0.08	0.16	0.21	0.27
Au	0.36	0.25					0.2	0.07	0.09	0.06
Th	0.43	0.53					0.16	0.14	0.28	0.35
U	0.2	0.11					0.06	0.03	0.09	0.08
<i>ICPMS (ppm)</i>										
V	32	32	48	21	30	34	38		45	36
Cr	2230	2830	2570	2380	1950	2380	3330		2430	2100
Co	93	95	115	72	119	89	104		104	117
Ni	1770	1770	2150	1430	2390	1550	1800		1830	2250
Zn	31	36	66	n.d.	48	41	53		49	51
Ga	1	1	1	2	1	1	2		2	2
Rb	4	3	4	3	n.d.	n.d.	n.d.		2	3
Sr	12	8	8	26	11	8	16		29	24
Ba	5	4	4	12	4	n.d.	3		8	11
Y	1	2	n.d.	4	n.d.	1	2		5	3
Zr	22	11	3	24	7	6	10		12	12
Nb	6	5	2	4	n.d.	n.d.	1		3	8
La	5.6	3.8	1.0	5.0	1.4	0.7	1.3		2.4	2.5
Ce	11.3	7.7	1.9	10.4	2.5	1.4	3.3		5.7	5.1
Pr	1.04	0.74	0.18	1.18	0.25	0.18	0.44		0.74	0.58
Nd	3.3	2.4	0.5	4.7	1.0	0.9	2.0		3.4	2.1
Sm	0.5	0.5	n.d.	0.9	0.2	0.2	0.5		0.8	0.4
Eu	0.13	0.08	n.d.	0.24	0.06	0.07	0.12		0.21	0.10
Gd	0.4	0.3	n.d.	0.8	0.2	0.2	0.4		0.7	0.4
Tb	n.d.	n.d.	n.d.	0.1	n.d.	n.d.	n.d.		0.1	n.d.
Dy	0.2	0.3	0.1	0.6	0.1	0.2	0.4		0.7	0.4
Ho	n.d.	n.d.	n.d.	0.1	n.d.	n.d.	n.d.		0.1	n.d.
Er	0.1	0.2	n.d.	0.4	n.d.	0.1	0.2		0.4	0.2
Tm	n.d.	n.d.	n.d.	0.06	n.d.	n.d.	n.d.		0.05	n.d.
Yb	0.1	0.2	n.d.	0.3	n.d.	n.d.	0.2		0.3	0.3
Lu	n.d.	n.d.	n.d.	0.05	n.d.	n.d.	n.d.		n.d.	n.d.
Hf	0.6	0.2	n.d.	0.5	n.d.	n.d.	0.3		0.3	0.2
Ta	0.3	0.3	n.d.	0.3	n.d.	n.d.	n.d.		0.2	0.2
Th	0.5	0.5	0.1	0.4	0.1	n.d.	0.1		0.3	0.4
U	0.1	0.1	n.d.	n.d.	n.d.	n.d.	n.d.		n.d.	0.1

Chemical zoning and the range in compositions observed among the different phases (Tables 5 and 7; Fig. 5) imply that metasomatic agents of different compositions may have been in operation.

The strong depletion in Zr–Hf and Ti relative to REE (Fig. 9) found among clinopyroxenes in Tenerife xenoliths is generally regarded as a strong indicator of carbonatite metasomatism (e.g. Rudnick *et al.*, 1994; Klemme *et al.*,

Rock:	HLCO					Spinel dunite		Spinel wehrlite	
Sample:	TF14-39	TF14-41	TF14-42	TF14-59	TF14-62	TF14-4	TF14-50	TF14-35	TF14-46
<i>XRF (wt %)</i>									
SiO ₂	42.46	42.12	40.85	42.43	42.40	43.58	38.61	41.09	42.54
TiO ₂	0.06	0.12	0.20	0.19	0.10	0.01	0.06	0.17	0.15
Al ₂ O ₃	0.60	0.66	0.83	0.84	0.76	0.61	0.71	0.61	0.86
FeO _{total}	8.08	8.45	8.74	10.09	9.29	7.89	11.02	8.62	8.64
MnO	0.17	0.18	0.46	0.23	0.44	0.13	0.17	0.44	0.44
MgO	44.97	44.95	44.60	41.87	43.28	45.53	44.95	44.15	42.14
CaO	1.52	1.47	1.45	2.36	1.68	0.70	1.37	2.98	2.82
Na ₂ O	0.23	0.15	0.18	0.14	0.17	0.12	0.12	0.14	0.24
K ₂ O	0.10	0.04	0.25	0.03	0.07	0.03	0.03	0.02	0.09
P ₂ O ₅	0.01	0.01	0.01	0.01	0.01	0.01	0.01	0.01	0.01
LOI	-0.11	-0.25	0.12	-0.56	-0.23	n.d.	0.08	-0.29	n.d.
Sum	98.09	98.66	97.68	97.63	97.96	98.61	97.13	97.94	97.93
<i>XRF (ppm)</i>									
V	47	42	34	63	77	46	82	47	37
Cr	3270	3000	3840	3120	3280	3320	4650	2340	2860
Co	116	117	119	109	112	116	146	118	116
Ni	2420	2430	2500	1970	2130	2460	2110	2410	2320
Zn	72	75	210	105	187	55	73	95	164
Rb	8	5	18	5	6	4	6	5	7
Sr	31	21	35	23	27	10	32	33	49
Y	4	n.d.	1	3	5	n.d.	n.d.	1	10
Zr	20	20	17	20	27	14	14	19	64
Nb	15	3	5	2	11	3	2	2	15
<i>INAA (ppm)</i>									
K	1200	308	2710	291	398	361	239	182	868
Na	2540	1910	2090	1830	1890	1540	1910	1790	2480
Sc	9.11	8.55	6.93	9.15	7.88	9.39	7.21	9.19	10.57
Ga	0.69	1.89	0.47	1.31	1.87	0.45	1.39	0.7	1.09
As	0.91	0.91	0.42	0.64	1.63	1.19	0.97	0.46	0.49
Ba	16.0	9.4	13.8	20.3	26.0	9.1	5.2	11.3	22.2
La	11.1	1.35	2.82	1.06	2.47	3.06	0.99	1.73	6.78
Ce	20	2.25	3.76	2.58	3.72	4.38	0.51	3.07	15.87
Nd	6.31	4.65	2.25	1.12	11.02	2.76	2.77	n.d.	2.37
Sm	1.53	0.72	0.61	0.92	1.45	0.43	0.28	0.89	2.39

1995; Coltorti *et al.*, 1999). Lherzolite xenoliths from Grande Comore, Indian Ocean, in which Zr–Hf–Ti-depleted clinopyroxenes are interpreted as the result of carbonatite metasomatism, also show growth of clinopyroxene at the expense of orthopyroxene, CaO/Al₂O₃ ratios \gg 1, and enrichment in incompatible trace elements and alkalis (Coltorti *et al.*, 1999). Ca metasomatism

is otherwise typically found in peridotite xenoliths in kimberlites (Boyd, 1996). It should be noticed that clinopyroxene-rich spinel lherzolites in many locations, e.g. Hawaii, have CaO/Al₂O₃ \sim 1.0, and have thus not been subjected to Ca metasomatism (Boyd, 1996). In a plot of (La/Yb)_N against Ti/Eu (Fig. 14) Tenerife clinopyroxenes form a trend from high Ti/Eu ratios and

Table 10: continued

Sample:	TF14-39	TF14-41	TF14-42	TF14-59	TF14-62	TF14-4	TF14-50	TF14-35	TF14-46
Eu	0.47	0.17	0.35	0.68	0.49	0.18	0.29	0.79	0.98
Gd	1.02	1.2	0.7	0.45	0.93	1.03	0.84	0.41	0.63
Tb	0.16	0.08	0.05	0.04	0.13	0.03	0.02	0.08	0.15
Ho	0.23	0.2	0.13	0.29	0.32	0.1	0.06	0.17	0.55
Yb	0.67	0.43	0.41	0.57	0.9	0.17	0.17	0.36	1.43
Hf	0.21	0.19	0.19	0.4	0.6	n.d.	0.14	0.33	1.23
Ta	0.34	0.07	0.19	0.09	0.71	0.03	0.03	0.1	1.35
Au	0.41	0.31	0.08	0.12	0.27	0.29	2.32	n.d.	0.15
Th	0.37	0.08	0.16	0.03	0.14	0.13	0.13	0.11	0.23
U	0.11	0.08	0.04	0.02	0.09	0.06	0.05	0.01	0.12
<i>ICPMS (ppm)</i>									
V	34	37	25	52	55	41	64		
Cr	2770	2910	3820	2930	3000	2950	4480		2270
Co	71	115	120	108	90	115	119		76
Ni	1340	2110	2320	1790	1480	2230	1610		1440
Zn	n.d.	70	187	100	165	51	46		69
Ga	2	2	3	2	3	1	2		3
Rb	4	n.d.	15	n.d.	3	n.d.	n.d.		3
Sr	26	19	33	20	24	8	28		40
Ba	9	6	28	5	11	4	n.d.		11
Y	6	4	3	6	8	2	1		11
Zr	13	14	13	12	19	7	5		48
Nb	10	2	3	n.d.	7	1	n.d.		9
La	11.2	1.4	3.2	1.2	2.9	3.2	1.1		6.9
Ce	24.8	3.8	6.4	3.9	7.5	7.1	2.3		19.5
Pr	2.67	0.58	0.73	0.64	1.04	0.72	0.30		2.62
Nd	9.4	2.8	3.0	3.2	5.0	2.4	1.2		11.1
Sm	1.4	0.8	0.7	0.9	1.4	0.4	0.3		2.2
Eu	0.32	0.17	0.17	0.26	0.33	0.11	0.08		0.49
Gd	1.1	0.7	0.5	0.9	1.2	0.3	0.2		2.0
Tb	0.2	0.1	n.d.	0.2	0.2	n.d.	n.d.		0.3
Dy	1.0	0.6	0.5	1.0	1.3	0.3	0.2		1.7
Ho	0.2	0.1	0.1	0.2	0.3	n.d.	n.d.		0.4
Er	0.5	0.4	0.3	0.6	0.8	0.2	0.1		1.2
Tm	0.09	0.07	0.06	0.09	0.11	n.d.	n.d.		0.20
Yb	0.5	0.4	0.4	0.6	0.8	0.2	0.1		1.3
Lu	0.08	0.07	0.08	0.09	0.13	n.d.	n.d.		0.21
Hf	0.3	0.3	0.3	0.4	0.6	n.d.	n.d.		1.5
Ta	0.3	0.1	0.2	n.d.	0.7	n.d.	n.d.		1.2
Th	0.4	0.1	0.2	n.d.	0.2	0.4	0.1		0.3
U	n.d.	n.d.	n.d.	n.d.	0.1	n.d.	n.d.		0.1

Major element compositions (XRF) are given in wt %. Trace element compositions obtained by XRF, INAA, and ICPMS are given in ppm. Data for the same element in a given sample, analysed by different methods, agree reasonably well. n.d., not detected. Definitions of HEXO, HTR and HLCO are given in the footnote to Table 2.

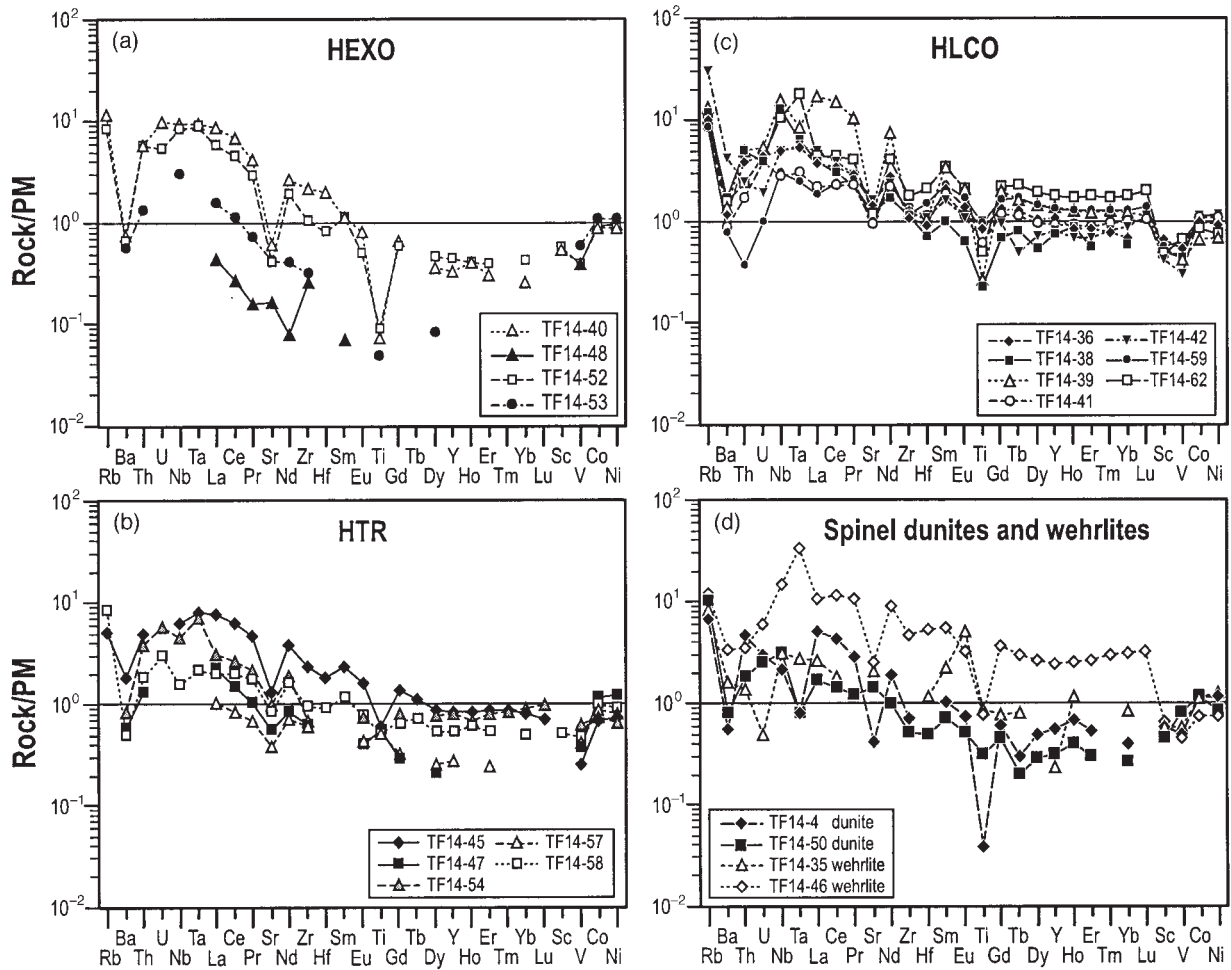


Fig. 9. Trace element concentrations in mantle xenoliths from Tenerife, normalized to primordial mantle (PM; from McDonough & Sun, 1995).

very low $(La/Yb)_N$ ratios typical of clinopyroxene in DMM, to the field of clinopyroxenes in mantle xenoliths believed to have been subjected to carbonatite metasomatism [very low Ti/Eu ratios and high $(La/Yb)_N$ ratios]. This strongly suggests carbonatitic melts as metasomatic agents in the upper mantle beneath Tenerife. Carbonatitic melts are frequently called upon to explain mantle metasomatism (e.g. Green & Wallace, 1988; Yaxley *et al.*, 1991; Green *et al.*, 1992; Hauri *et al.*, 1993; Ionov *et al.*, 1993; Chalot-Prat & Arnold, 1999).

To test the hypothesis of metasomatism caused by carbonatite melt(s), we have used the trace element compositions of clear clinopyroxene cores in HLCO xenoliths together with published cpx–melt partition coefficients (Table 12) to estimate the trace element compositions of fluids or melts in equilibrium with this clinopyroxene. The partitioning of elements between

melts and minerals depends strongly upon the composition of the melt. We therefore had to define the types of melts for which estimates should be made. In addition to carbonatitic melts suggested by the trace element compositions of clinopyroxene, two types of silicate melts seem indicated as potential metasomatic agents: basaltic melts and silicic melts. The extensive alkali basaltic magmatism in Tenerife (and the other Canary Islands) implies that alkali basaltic melts have ascended through the lithospheric mantle. Metasomatism by alkali basaltic melts is therefore possible. Silicic glasses (51–69 wt % SiO_2) are abundant in the Tenerife xenoliths, both as inclusions and as interstitial glass pockets (Neumann & Wulff-Pedersen, 1997; Table 9), and it has been proposed that alkali–silica-rich, Ti–Mg–Ca–P-poor melts ($SiO_2 > 60$ wt %) percolating through the mantle may represent important metasomatic agents (Zinngrebe & Foley, 1995;

Table 11: Sr–Nd isotope compositions of different types of whole-rock mantle xenoliths, and clinopyroxene separates from spinel harzburgite and lherzolite xenoliths

	$^{87}\text{Sr}/^{86}\text{Sr}$	2 σ	$^{143}\text{Nd}/^{144}\text{Nd}$	2 σ
<i>Clinopyroxene separates</i>				
TF14-2 HCLO	0.703142	11	0.512911	7
	0.703116	25		
TF14-5 HCLO	0.703234	13	0.512928	9
	0.703189	17	0.512900	7
TF14-41 HCLO	0.703155	10	0.512911	7
<i>Whole rocks</i>				
TF14-59 HCLO	0.703141	9	0.512876	7
TF14-46 wehrlite	0.703139	17	0.512954	11
TF14-51 clinopyroxenite	0.703136	13	0.512915	11
TF14-55 clinopyroxenite	0.703121	11	0.512871	8

All data are normalized to $^{87}\text{Sr}/^{86}\text{Sr} = 0.71025$ for the NBS 987 Sr standard. Data on two clinopyroxenites are included for comparison.

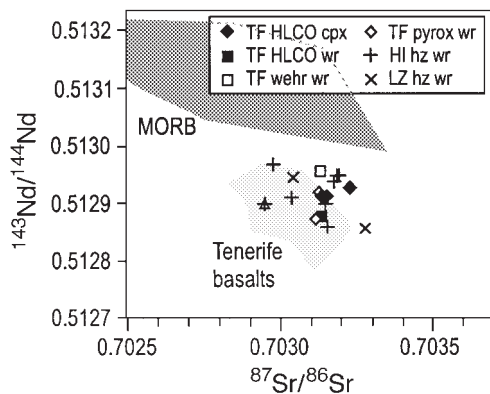


Fig. 10. Sr–Nd isotope compositions of clinopyroxene separates in HLCO spinel harzburgites and lherzolites (cpx) and whole-rock data on harzburgites and lherzolites (wr), spinel wehrlites (wehr wr) and clinopyroxenites (pyrox wr). For comparison are shown data on spinel harzburgite xenoliths from Hierro and Lanzarote (HI hz wr and LZ hz wr, respectively; Whitehouse & Neumann, 1995), the field of basaltic lavas from Tenerife (Simonsen *et al.*, 2000), and part of the MORB field (Ito *et al.*, 1987). Analytical error is within the size of the symbols.

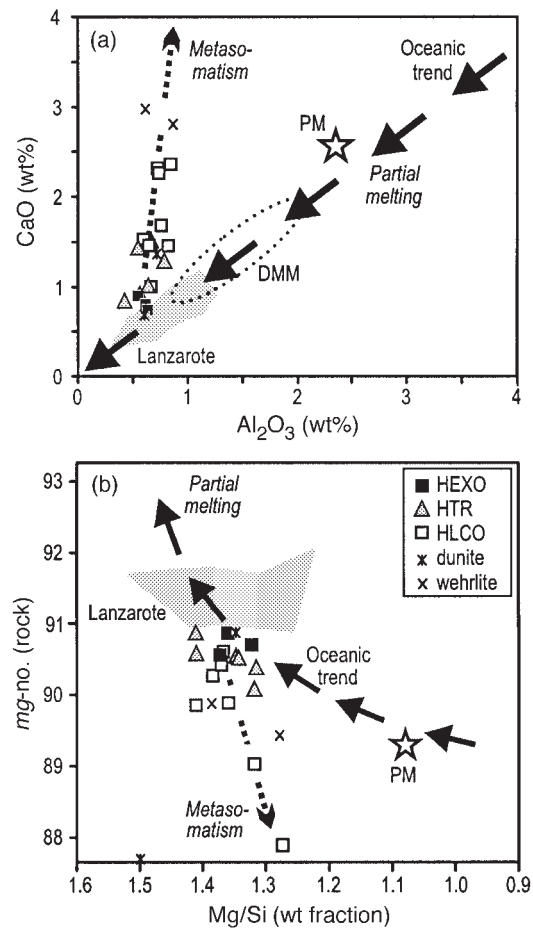


Fig. 11. (a) CaO–Al₂O₃, and (b) mg-number–Mg/Si relations in mantle xenoliths from Tenerife, compared with the oceanic trend, and field of DMM of Boyd (1996), and the field of spinel harzburgites and lherzolites from Lanzarote [data from Siena *et al.* (1991) and Neumann *et al.* (1995)].

Wulff-Pedersen *et al.*, 1996; Draper & Green, 1997; Neumann & Wulff-Pedersen, 1997).

The partition coefficients $D^{\text{cpx/melt}}$ in mantle systems appear to increase significantly with increasing SiO₂ content or increasing degree of polymerization of the melt (Neumann & Wulff-Pedersen, 1997; Vannucci *et al.*, 1998), in a similar manner to the relations shown for basaltic to highly silicic magmas (e.g. Green & Pearson, 1985; Sisson, 1991; Green, 1994). We therefore use two sets of partition coefficients to estimate the trace element compositions of silicate melts in equilibrium with clinopyroxene in HLCO xenoliths; one set (low- D) is relevant for melts of basaltic composition, the other (high- D) for silicic melts (SiO₂ >60 wt %).

Alkali basaltic melts

PM-normalized trace element patterns of basaltic melts estimated on the basis of low- $D^{\text{cpx/melt}}$ (data from Hart &

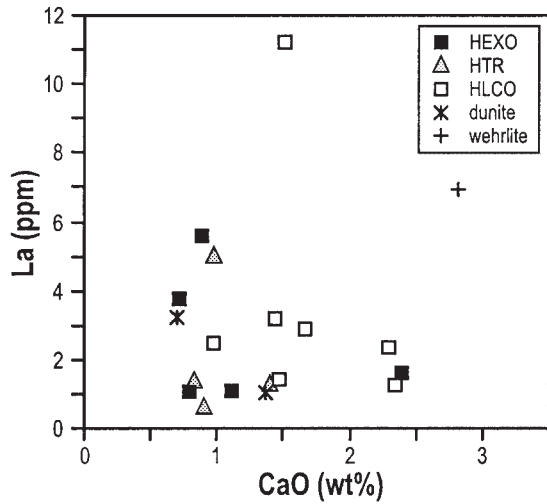


Fig. 12. Whole-rock concentrations of La plotted against CaO, showing that Ca metasomatism and trace element enrichment are not correlated.

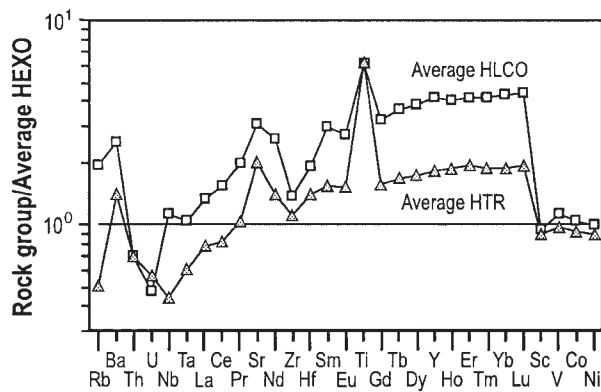


Fig. 13. Average trace element compositions of HLCO and HTR normalized to those of average HEXO. For elements missing from the HEXO and HTR datasets because of concentrations below the detection limits, values were interpolated to form trace element patterns parallel to those exhibited by complete datasets. Sample TF14-48 was omitted from the HEXO-average as about half the trace element concentrations were below the detection limit (Table 10), implying that the estimated average is higher than the true one. We believe, however, that the general shape of the pattern is representative. (See text for comments and interpretation.)

Dunn, 1993; Salters & Longhi, 1999; Green *et al.*, 2000) are shown in Fig. 15a. The estimated trace element patterns differ markedly from those exhibited by aphyric basaltic lavas in Tenerife (Neumann *et al.*, 1999). Furthermore, the extremely low Al–Ti contents of many pyroxenes in HLCO are not compatible with formation through reactions between harzburgite and alkali basaltic melts; the latter typically being Ti–Al rich (e.g. Wulff-Pedersen *et al.*, 1996). We conclude that it is highly unlikely that the metasomatism was caused by basaltic magmas.

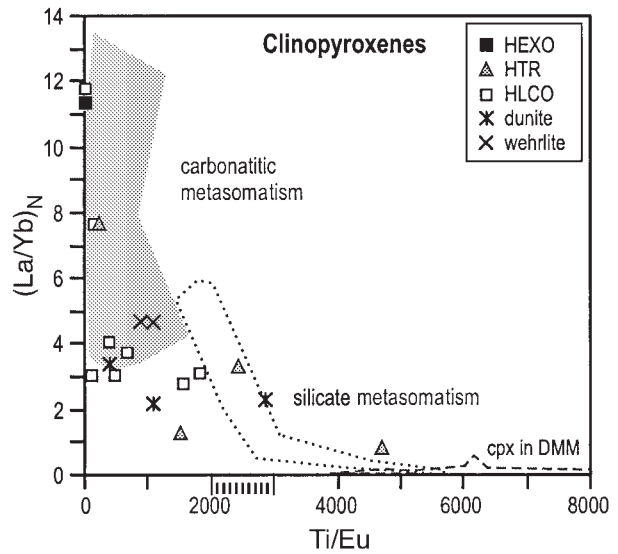


Fig. 14. $(La/Yb)_N$ plotted against Ti/Eu for clinopyroxenes in mantle xenoliths from Tenerife. For comparison are plotted the fields of clinopyroxenes in ultramafic xenoliths believed to have been subjected to carbonatitic (light grey field) and silicate (dotted line) metasomatism (Coltorti *et al.*, 1999, and references therein), and the field (dashed line) of clinopyroxenes in DMM (Ti/Eu: 3900–12 700; data from Johnson *et al.*, 1990; Johnson & Dick, 1992).

High-silica melts

Silicate melt compositions estimated on the basis of high- $D_{cpx/melt}$ determined for peridotites (Ionov *et al.*, 1994; Chazot *et al.*, 1996) have PM-normalized trace element patterns (Fig. 15b) that fall in the general area of analysed silicic glasses in Tenerife xenoliths, but their strong negative anomalies for P, Zr–Hf, and Ti are not matched by the natural glasses. Silicic melts thus seem unlikely as the metasomatic agents.

Carbonatitic melts

Carbonatite melt compositions estimated on the basis of cpx–carbonatite partition coefficients (Klemme *et al.*, 1995, for V and Ni; Adam & Green, 2001) are shown in Fig. 15c. The estimated patterns fall essentially within the range of average carbonatites, as given by Woolley & Kempe (1989). Carbonatitic melts at mantle pressures are highly enriched in LREE, P, Na, K, Sr, and Rb, and effective in fractionating these elements relative to high field strength elements (e.g. Green & Wallace, 1988; Yaxley *et al.*, 1991, 1998; Hauri *et al.*, 1993; Ionov *et al.*, 1993). The estimated trace element patterns show the predicted negative anomalies for Zr, Hf, and Ti, but the enrichment in LREE relative to HREE is somewhat lower than expected for natural carbonatite magmas. The estimated melts are also very depleted in Ba relative

Table 12: Partition coefficients for cpx/melt used to estimate the trace element compositions of melts in equilibrium with clinopyroxenes in highly metasomatized mantle xenoliths from Tenerife

	Cpx/silicate melt		Cpx/carb. melt
	low <i>D</i>	high <i>D</i>	
Rb	0.07	0.071	0.006
Ba	0.0007	0.0006	0.07
Th	0.007	0.007	0.004
U	0.008	0.005	0.004
Nb	0.045	0.01	0.10
Ta	0.04	0.01	0.15
La	0.10	0.26	0.07
Ce	0.11	0.33	0.09
Pr	0.14	0.43	0.11
Sr	0.11	0.15	0.08
Nd	0.19	0.64	0.11
Zr	0.14	0.3	0.48
Hf	0.24	0.23	0.16
Sm	0.32	0.95	0.13
Eu	0.35	1.02	0.22
Ti	0.38	0.71	1.4
Gd	0.35	1.1	0.26
Tb	0.38	1.1	0.28
Dy	0.40	0.97	0.29
Y	0.54	1.10	0.30
Ho	0.43	0.91	0.29
Er	0.44	0.83	0.29
Tm	0.47	1.04	0.29
Yb	0.50	1.07	0.29
Lu	0.5	1.07	0.29
Sc	1.3	10	
V	3.1	1.6	2.9
Co		2.3	
Ni			1.7

'Low *D*' values represent partitioning of elements between clinopyroxene and basaltic melts determined experimentally by Hart & Dunn (1993), Salters & Longhi (1999) and Green *et al.* (2000). 'High *D*' values, representing partitioning between Cr-diopside and highly silicic melts (SiO₂ >60 wt %) in peridotites, are based on data published by Ionov *et al.* (1994) and Chazot *et al.* (1996). For clinopyroxene-carbonatitic magma we use partition coefficients published by Adam & Green (2001) for all elements except V and Ni, for which are used data by Klemme *et al.* (1995).

to natural carbonatites (Fig. 15c). However, metasomatism by carbonatitic melts may easily account for the formation of clinopyroxene at the expense of

orthopyroxene. Experimental studies on reactions between carbonatite melts and peridotite have shown that at pressures below 2.1 GPa, enstatite (in lherzolite or harzburgite) will be replaced by clinopyroxene + olivine ± chromite (e.g. Meen, 1987; Green & Wallace, 1988; Yaxley & Green, 1996). Furthermore, experimental and empirical data indicate that carbonatite metasomatism decreases the Al content of the orthopyroxene, decreases Al and Ti and increases Na and Cr in the clinopyroxene, and increases the Cr/(Cr + Al) ratio of spinel (e.g. Green & Wallace, 1988; Yaxley *et al.*, 1991, 1998; Yaxley & Green, 1996; Chalot-Prat & Arnold, 1999), although studies by Ionov (1998) and E. van Achterbergh (personal communication, 2001) show the opposite relationship. The Al-Ti-poor, Na-Cr-rich clinopyroxenes in Tenerife xenoliths (Table 5) are thus in agreement with formation in the presence of carbonatitic melts. Finally, the associations of CO₂ with silicate glass and/or silicate daughter minerals observed in many fluid inclusions from Tenerife suggest the presence of silicic carbonatite melts in the upper mantle beneath Tenerife (Neumann *et al.*, 2000; Viti & Frezzotti, 2002). All the evidence taken together makes silicic carbonatite melts by far the most likely metasomatic agent in the upper mantle beneath Tenerife.

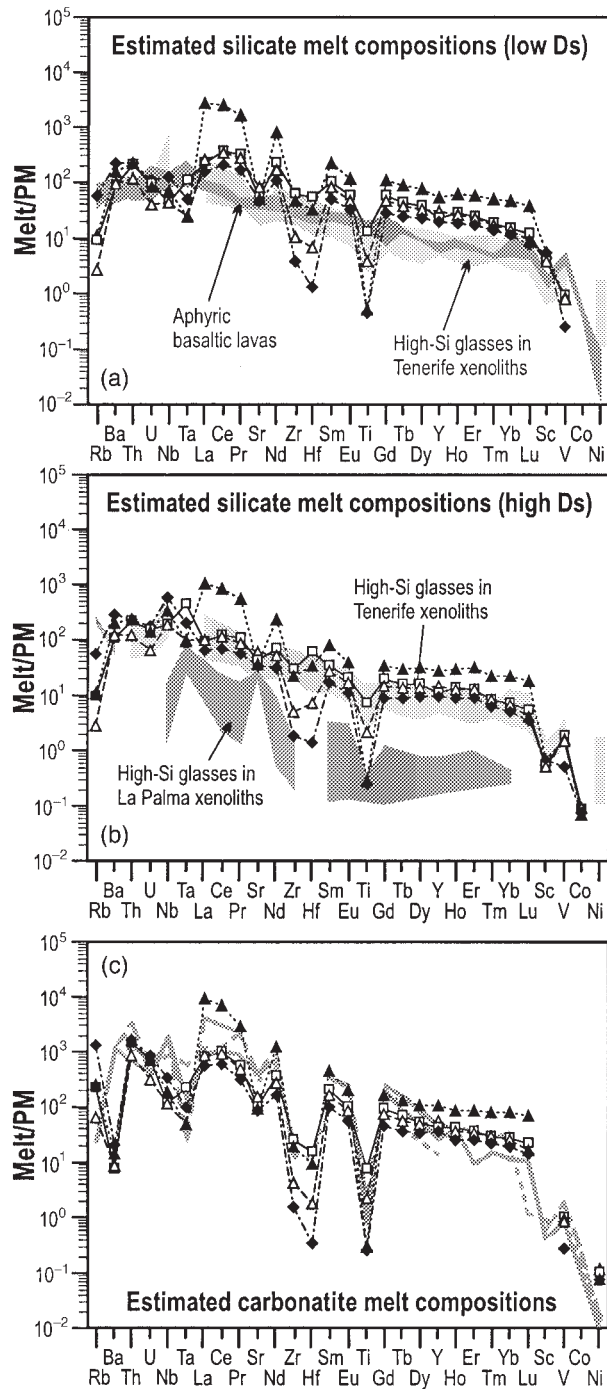
The observed range in clinopyroxene compositions within single samples implies a range in compositions in the melts from which they formed. This is reflected in the melt estimates (Fig. 15). The mineral zoning patterns (Tables 5 and 7; Fig. 6) suggest increasing Al-Ti concentrations with time in the metasomatizing melts. As the lowest Ti concentrations are found among the most REE-Sr-Zr-Hf-depleted clinopyroxenes (and associated melts), the clinopyroxene zoning patterns indirectly imply progressively increasing REE contents, increasing LREE/HREE ratios, and decreasing degree of depletion in Zr, Hf and Ti in the metasomatizing melts. Changes in the compositions of the metasomatizing melts may arise from different types of fluid-wall-rock interaction at deeper levels in the mantle (e.g. different phase assemblages), or, more likely, reflect a change in the type of melts produced by the Canary Islands plume, from carbonatitic towards basaltic ones. Because of their complexity, we have made no attempt to model the metasomatic processes.

The origin of dunites and wehrlites

Both the whole-rock and mineral chemistry of the dunites and wehrlites show clear affinity to the HLCO and HTR with respect to mineral chemistry (e.g. high enrichment in REE, enrichment in LREE relative to HREE, and strong depletion in Zr-Hf and Ti relative to REE in clinopyroxene; Tables 2, 3 and 5-8; Figs 4 and 7).

Estimated trace element compositions of melts in equilibrium with clinopyroxenes in these rocks (based on clinopyroxene compositions and cpx–melt distribution coefficients) fall within the range of those estimated on the basis of Cr-diopside in HLCO xenoliths (not shown), implying a carbonatitic melt as the most likely metasomatic agent. It thus seems likely that these rocks have

been through similar processes as the harzburgites and lherzolites. Minor amounts of orthopyroxene present in some rocks are interpreted as remnants from the original ol + opx ± cpx ± sp assemblage, altered to the assemblage ol + cpx ± opx ± sp through metasomatic reactions. Like HLCO, the dunites and wehrlites have lower *mg*-numbers than HEXO, also a natural result of the metasomatism. Trapping by spinel may explain relatively high Nb and Ta contents in wehrlite TF14-46 (Fig. 9).



Sr–Nd isotopic relationships

Like mantle xenoliths from other Canary Islands (Whitehouse & Neumann, 1995), the Tenerife xenoliths and clinopyroxene separates have Sr–Nd isotopic compositions closely similar to those of Tenerife basalts, and fall well outside the MORB field (Fig. 10). Three explanations are possible: (1) the Sr–Nd composition of the upper mantle beneath Tenerife was reset by ascending Canary Islands basalt melts (e.g. Whitehouse & Neumann, 1995); (2) the basaltic lavas are contaminated by metasomatized lithospheric mantle [proposed by Zhang *et al.* (2001) for the upper mantle beneath North Queensland]; or (3) the metasomatizing melts and the basaltic melts have initially the same isotopic composition. Silicic carbonatite melts are believed to have caused the metasomatism in the upper mantle beneath Tenerife. It seems highly unlikely that basaltic melts would cause isotopic resetting without affecting the trace element geochemistry. Hypothesis (1) is therefore discarded. Hypothesis (2) implies that the silicic carbonatite metasomatism preceded the basalt volcanism, opening the possibility that the metasomatism and the basalt volcanism represent two unrelated events. This is possible, but it seems unlikely that the basaltic melts have been totally reset with respect to isotopic compositions without leaving evidence of chemical interaction in the mantle rocks. The most likely

Fig. 15. Estimated trace element compositions of silicic and carbonatitic melts which may have acted as metasomatic agents in the upper mantle under Tenerife. The compositions are calculated on the basis of: (a) clinopyroxene–melt partition coefficients ($D^{\text{cpx/melt}}$) relevant for basaltic melts; (b) $D^{\text{cpx/melt}}$ relevant for partitioning of elements between highly silicic melts and mantle minerals; (c) $D^{\text{cpx/melt}}$ for carbonatite melt. Partition coefficients and references are given in Table 12. The results are shown for four clinopyroxenes in HLCO xenoliths (see Table 6): the least REE-rich one (TF14-38-I: \blacklozenge); the most REE-rich one (TF14-39: \blacktriangle); the most Ti-rich one (TF14-59-I: \square); an average-type clinopyroxene (TF14-38-I: \triangle). The estimated melt compositions are compared with aphyric basaltic lavas in Tenerife (Neumann *et al.*, 1999), silicate glasses in Tenerife xenoliths (56–63 wt % SiO_2 ; Table 10) and La Palma xenoliths (~ 68 wt % SiO_2 ; E.-R. Neumann, unpublished data, 2000), and average carbonatites (Woolley & Kempe, 1989).

explanation is model (3), implying that the metasomatizing melts and the basaltic magmas have similar isotopic compositions, both originating in the Canary Islands plume.

Sequence of events

We have shown above that in the upper mantle beneath Tenerife metasomatism was superimposed on strongly depleted mantle rocks. Depleted orthopyroxene in HEXO and HLCO may have survived the metasomatism. Strong depletion followed by metasomatism also characterizes mantle xenoliths from Lanzarote (Siena *et al.*, 1991; Neumann *et al.*, 1995). The high degree of partial melting reflected in mantle xenoliths from Tenerife and Lanzarote may be associated with the opening of the Central Atlantic Ocean. A widespread tholeiitic magmatic event at ~200 Ma along the passive continental margins of the Central Atlantic Ocean is believed to be plume related (Wilson & Guiraud, 1998, and references therein). The plume activity may have generated a more than average depleted oceanic lithosphere in the area because of higher degrees of partial melting. However, strong depletion overprinted by metasomatism appears to be a common feature in ocean islands. Other examples include Savai'i in Western Samoa (Hauri & Hart, 1994) and Kerguelen (e.g. Mattielli *et al.*, 1996; Grégoire *et al.*, 2000). Mattielli *et al.* (1996) and Grégoire *et al.* (2000) proposed that in Kerguelen the strong depletion results from a pre-metasomatic partial melting process caused by the Kerguelen plume. An alternative explanation is therefore that at the onset of the Canary Islands magmatic event, old, 'normal' Central Atlantic mantle lithosphere was subjected to a second period of partial melting and depletion as a result of heating at the base of the lithosphere by the Canarian plume. Partial melting and depletion of the mantle lithosphere gave way to metasomatism as fluids or melts started to rise through the lithospheric mantle. It is likely that the continuing basalt volcanism in Tenerife post-dates the main metasomatic event.

CONCLUSIONS

(1) The lithospheric mantle beneath Tenerife has suffered extensive partial melting and strong depletion (stronger than 'normal' depleted MORB mantle), followed by metasomatism.

(2) The 'higher-than-normal' degree of partial melting in the upper mantle beneath Tenerife (and other Canary Islands) is probably associated with plume activity in the area during the opening of the Central Atlantic Ocean. An alternative possibility is that the oceanic lithosphere beneath the Canary Islands went through a second

episode of partial melting in response to heating at an early stage of the Canary Islands magmatic event.

(3) The metasomatism comprises recrystallization of orthopyroxene porphyroclasts with a tight system of exsolution lamellae into 'clear', poikilitic orthopyroxene porphyroclasts (no visible exsolution lamellae), formation of olivine and REE–Cr-rich, strongly Zr–Hf–Ti-depleted clinopyroxene at the expense of orthopyroxene, formation of minor amounts of phlogopite, decreasing *mg*-numbers, addition of highly incompatible trace elements, and increased whole-rock CaO/Al₂O₃ ratios to values >> 1 (Ca metasomatism).

(4) The metasomatism was caused by silicic carbonatite melts. The composition of the metasomatizing melts changed with time, possibly as the result of changing compositions of the melts produced in the Canary Islands plume.

(5) The metasomatism mainly acted as an open-system process, meaning that a metasomatic agent ascending through the upper mantle caused reactions and chemical exchange between fluid and wall-rock, leaving a residual fluid, which moved to shallower levels. Elements compatible with the wall-rock minerals and/or with phases formed through metasomatic reactions (clinopyroxene and phlogopite) were 'trapped' by these minerals, whereas elements incompatible with all the phases in the metasomatized rocks were preferentially transported away by the residual fluid.

(6) Spinel dunites and wehrlites formed in response to extensive metasomatic processes, similar to those described for the spinel harzburgites and lherzolites, consuming most or all of the orthopyroxene.

(7) Peridotites and clinopyroxene separates have Sr–Nd isotopic compositions closely similar to those of Tenerife basalts. This indicates resetting from the expected original MORB composition by the metasomatizing fluids. It is likely that the metasomatizing carbonatitic melts represent an early phase of partial melting in the mantle plume, which also gives rise to the exposed basaltic lavas.

ACKNOWLEDGEMENTS

We thank Dr Joan Martí for help to obtain permits for sampling and exporting rocks in Tenerife. Drs Françoise Chalot-Prat, Michel Grégoire, Bill Griffin, John Lassiter, Sue O'Reilly and Marge Wilson are thanked for suggestions and constructive criticism of earlier versions of this paper. Muriel Erambert, Toril Enger, Mélanie Griselin, Ashwini Sharma and Gareth Davies are gratefully acknowledged for help with the analytical work. Fieldwork in Tenerife was made very pleasant because of the good accommodation at the Parador de Cañadas del Teide, and efforts of the friendly staff there. We are

grateful to the GEMOC Key Centre for teaching E. Wulff-Pedersen and E.-R. Neumann to use analytical equipment as part of the GEMOC international exchange activities. This project was supported by grants from the Norwegian Research Council (NFR) and from the Commission of the European Communities, DGXII, Environment Programme, Climatology and Natural Hazards Unit, under contract EV5V-CT-9283.

REFERENCES

- Abdel-Monem, A., Watkins, N. D. & Gast, P. W. (1971). Potassium–argon ages, volcanic stratigraphy, and geomagnetic polarity history of the Canary Islands: Lanzarote, Fuerteventura, Gran Canaria, and La Gomera. *American Journal of Science* **271**, 490–521.
- Abdel-Monem, A., Watkins, N. D. & Gast, P. W. (1972). Potassium–argon ages, volcanic stratigraphy, and geomagnetic polarity history of the Canary Islands: Tenerife, La Palma and Hierro. *American Journal of Science* **272**, 805–825.
- Adam, J. & Green, T. H. (2001). Experimentally determined partition coefficients for minor and trace elements in peridotite and carbonatitic melts, and their relevance to natural carbonatites. *European Journal of Mineralogy* **13**, 815–827.
- Andersen, T., O'Reilly, S. Y. & Griffin, W. L. (1984). The trapped fluid phase in upper mantle xenoliths from Victoria, Australia: implications for mantle metasomatism. *Contributions to Mineralogy and Petrology* **88**, 72–85.
- Blundy, J. D., Robinson, J. A. C. & Wood, B. J. (1998). Heavy REE are compatible in clinopyroxene on the spinel lherzolite solidus. *Earth and Planetary Science Letters* **160**, 493–504.
- Bonatti, E., Peyve, A., Kepezhinskas, P., Kurentsova, N., Seyler, M., Skolotnev, S. & Udintsev, G. (1992). Upper mantle heterogeneity below the Mid-Atlantic Ridge, 0°–15°N. *Journal of Geophysical Research* **97**, 4461–4476.
- Boyd, F. R. (1996). Origin of peridotite xenoliths: major element considerations. In: Ranalli, G., Lucchi, F. R., Ricci, C. A. & Trommsdorff, T. (eds) *High Pressure and High Temperature Research on Lithosphere and Mantle Materials*. Siena: University of Siena, pp. 89–106.
- Brenan, J. M., & Watson, E. B. (1991). Partitioning of trace elements between carbonatitic melts and clinopyroxene and olivine at mantle *P–T*-conditions. *Geochimica et Cosmochimica Acta* **55**, 2203–2214.
- Brunfelt, A. O. & Steinnes, E. (1969). Instrumental activation analysis of silicate rocks with epithermal neutrons. *Analytica Chimica Acta* **48**, 13–24.
- Chalot-Prat, F. & Arnold, M. (1999). Immiscibility between calcio-carbonatitic and silicate melts and related wall rock reactions in the upper mantle: a natural case study from Romanian mantle xenoliths. *Lithos* 627–659.
- Chazot, G., Menzies, M. A. & Harte, B. (1996). Determination of partition coefficients between apatite, clinopyroxene, amphibole, and melt in natural lherzolites from Yemen: implications for wet melting in the lithospheric mantle. *Geochimica et Cosmochimica Acta* **60**, 423–437.
- Coltorti, M., Bonadiman, C., Hinton, R. W., Siena, F. & Upton, B. G. J. (1999). Carbonatite metasomatism of the oceanic upper mantle: evidence from clinopyroxenes and glasses in ultramafic xenoliths of Grande Comore, Indian Ocean. *Journal of Petrology* **40**, 133–165.
- Draper, D. S. & Green, T. H. (1997). Anhydrous and C–O–H fluid-saturated *PT* phase relations of silicic, alkaline, aluminous mantle-xenolith glasses. *Journal of Petrology* **38**, 1187–1224.
- Eggs, S. M., Rudnick, R. L. & McDonough, W. F. (1998). The composition of peridotites and their minerals: a laser-ablation ICP-MS study. *Earth and Planetary Science Letters* **154**, 53–71.
- Foley, S. F., Jackson, B. J., Greenough, J. D. & Jenner, G. A. (1996). Trace element partition coefficients from clinopyroxene and phlogopite in an alkaline lamprophyre from Newfoundland by LAM-ICP-MS. *Geochimica et Cosmochimica Acta* **60**, 629–638.
- Frezzotti, M. L., Andersen, T., Neumann, E.-R. & Simonsen, S. L. (2002). Carbonatite melt/CO₂ fluid connection in mantle xenoliths from Tenerife, Canary Islands. *Lithos* (submitted).
- Garrido, C. J., Bodinier, J.-L. & Alard, O. (2000). Incompatible trace element partitioning and residence in anhydrous peridotites and websterites from the Ronda orogenic peridotite. *Earth and Planetary Science Letters* **181**, 341–358.
- Glaser, S. M., Foley, S. F. & Guenther, D. (1999). Trace element compositions of minerals in garnet and spinel peridotite xenoliths from the Vitim volcanic field, Transbaikalia, eastern Siberia. *Lithos* **48**, 263–285.
- Govindaraju, K. (1989). Compilation of working values and sample descriptions for 272 geostandards. *Geostandards Newsletter* **13**, Special Issue, 1–113.
- Green, D. H. & Wallace, M. E. (1988). Mantle metasomatism by ephemeral carbonatite melts. *Nature* **336**, 459–462.
- Green, T. H. (1994). Experimental studies of trace element partitioning applicable to igneous petrogenesis—Sedona 16 years later. *Chemical Geology* **117**, 1–36.
- Green, T. H. & Pearson, N. J. (1985). Rare earth element partitioning between clinopyroxene and silicate liquid at moderate to high pressures. *Contributions to Mineralogy and Petrology* **91**, 24–36.
- Green, T. H., Adam, J. & Sie, S. H. (1992). Trace element partitioning between silicate minerals and carbonatite at 25 kbar and application to mantle metasomatism. *Mineralogy and Petrology* **46**, 179–184.
- Green, T. H., Blundy, J. D., Adam, J. & Yaxley, G. M. (2000). SIMS determination of trace element partition coefficients between garnet, clinopyroxene and hydrous basaltic liquids at 1–7.5 GPa and 1080–1200°C. *Lithos* **53**, 165–187.
- Grégoire, M., Moine, B. N., O'Reilly, S. Y., Cottin, J. Y. & Giret, A. (2000). Trace element residence and partitioning in mantle xenoliths metasomatized by highly alkaline, silicate- and carbonatite-rich melts (Kerguelen Islands, Indian Ocean). *Journal of Petrology* **41**, 447–509.
- Griffin, W. L., Shee, S. R., Ryan, C. G., Win, T. T. & Wyatt, B. A. (1999). Harzburgite to lherzolite and back again: metasomatic processes in ultramafic xenoliths from the Wesselton kimberlite, Kimberley, South Africa. *Contributions to Mineralogy and Petrology* **134**, 232–250.
- Hart, S. R. & Dunn, T. (1993). Experimental cpx/melt partitioning of 24 trace elements. *Contributions to Mineralogy and Petrology* **113**, 1–8.
- Hauri, E. H. & Hart, S. R. (1994). Constraints on melt migration from mantle plumes: a trace element study of peridotite xenoliths from Savai'i, Western Samoa. *Journal of Geophysical Research* **99**, 24031–24321.
- Hauri, E. H., Shimizu, N., Dieu, J. J. & Hart, S. R. (1993). Evidence for hotspot-related carbonatite metasomatism in the oceanic upper mantle. *Nature* **365**, 221–227.
- Hoernle, K. (1998). Geochemistry of Jurassic oceanic crust beneath Gran Canaria (Canary Islands): implications for crustal recycling and assimilation. *Journal of Petrology* **39**, 859–880.
- Ionov, D. (1998). Trace element composition of mantle-derived carbonates and coexisting phases in peridotite xenoliths from alkali basalts. *Journal of Petrology* **39**, 1931–1941.
- Ionov, D. A., Dupuy, C., O'Reilly, S. Y., Kopylova, M. G. & Genshaft, Y. S. (1993). Carbonated peridotite xenoliths from Spitsbergen:

- implications for trace element signature of mantle carbonate metasomatism. *Earth and Planetary Science Letters* **119**, 283–297.
- Ionov, D. A., Hofmann, A. W. & Shimizu, N. (1994). Metasomatism-induced melting in mantle xenoliths from Mongolia. *Journal of Petrology* **35**, 753–785.
- Ito, E., White, W. M. & Göpel, C. (1987). The O, Nd and Pb isotope geochemistry of MORB. *Chemical Geology* **62**, 157–176.
- Jaques, A. L. & Green, D. H. (1980). Anhydrous melting of peridotites at 0–15 kb pressure and the genesis of tholeiitic basalts. *Contributions to Mineralogy and Petrology* **73**, 287–310.
- Jensen, B. B. (1973). Patterns of trace element partitioning. *Geochimica et Cosmochimica Acta* **37**, 2227–2242.
- Johnsen, K. (1990). The nature and evolution of the lithosphere beneath Lanzarote, Canary Islands: evidence from upper mantle xenoliths. Candidatus Scientiarum thesis, University of Oslo, 106 pp.
- Johnson, K. T. M., & Dick, H. J. B. (1992). Open system melting and temporal and spatial variation of peridotite and basalt at the Atlantis II Fracture Zone. *Journal of Geophysical Research* **97**, 9219–9241.
- Johnson, K. T. M., Dick, H. J. B. & Shimizu, N. (1990). Melting in the oceanic upper mantle: an ion microprobe study of diopsides in abyssal peridotites. *Journal of Geophysical Research* **95**, 2661–2678.
- Klemme, S., van der Laan, S. R., Foley, S. F. & Günther, D. (1995). Experimentally determined trace and minor element partitioning between clinopyroxene and carbonatite melt under upper mantle conditions. *Earth and Planetary Science Letters* **133**, 439–448.
- LaTourette, T. Z. & Burnett, D. S. (1992). Experimental determination of U and Th partitioning between clinopyroxene and natural and synthetic basalt liquid. *Earth and Planetary Science Letters* **110**, 227–244.
- Mattielli, N., Weis, D., Gregoire, M., Mennessier, J. P., Cottin, J. Y. & Giret, A. (1996). Kerguelen basic and ultrabasic xenoliths; evidence for long-lived Kerguelen hotspot activity. In: Ludden, J. N., Arndt, N. T. & Francis, D. (eds) *Mafic Magmatism through Time*. *Lithos* **37**, 261–280.
- McDonough, W. F. & Sun, S.-s. (1995). The composition of the Earth. *Chemical Geology* **120**, 223–253.
- Mearns, E. W. (1986). Sm–Nd ages of Norwegian garnet peridotite. *Lithos* **19**, 269–278.
- Meen, J. K. (1987). Mantle metasomatism and carbonatites; an experimental study of a complex relationship. In: Morris, E. M. & Pasteris, J. D. (eds) *Mantle Metasomatism and Alkaline Magmatism*. *Geological Society of America, Special Paper* **215**, 91–100.
- Nash, W. P. & Crecraft, H. R. (1985). Partition coefficients for trace elements in silicic magmas. *Geochimica et Cosmochimica Acta* **49**, 2309–2322.
- Navon, O. & Stolper, E. (1987). Geochemical consequences of melt percolation; the upper mantle as a chromatographic column. *Journal of Geology* **95**, 285–307.
- Neumann, E.-R. (1991). Ultramafic and mafic xenoliths from Hierro, Canary Islands: evidence for melt infiltration in the upper mantle. *Contributions to Mineralogy and Petrology* **106**, 236–252.
- Neumann, E.-R. & Wulff-Pedersen, E. (1997). The origin of highly silicic glass in mantle xenoliths from the Canary Islands. *Journal of Petrology* **38**, 1513–1539.
- Neumann, E.-R., Sundvoll, B. & Overli, P. E. (1990). A mildly depleted upper mantle beneath southeast Norway: evidence from basalts in the Permo-Carboniferous Oslo Rift. In: Neumann, E.-R. (ed.) *Rift Zones in the Continental Crust of Europe—Geophysical, Geological and Geochemical Evidence: Oslo–Horn Graben*. *Tectonophysics* **178**, 89–107.
- Neumann, E.-R., Johnsen, K., Wulff-Pedersen, E. & Krogh, E. (1995). Petrogenesis of spinel harzburgite and dunite suite xenoliths from Lanzarote, eastern Canary Islands: implications for the upper mantle. *Lithos* **35**, 83–107.
- Neumann, E.-R., Wulff-Pedersen, E., Simonsen, S. L., Pearson, N. J., Mitjavila, J. & Martí, J. (1999). Evidence for fractional crystallization of periodically refilled magma chambers in Tenerife, Canary Islands. *Journal of Petrology* **40**, 1089–1123.
- Neumann, E.-R., Sørensen, V., Simonsen, S. L. & Johnsen, K. (2000). Gabbroic xenoliths from La Palma, Tenerife and Lanzarote, Canary Islands: evidence for reactions between Canary Islands melts and old oceanic crust. *Journal of Volcanology and Geothermal Research* **103**, 313–342.
- Norman, M. D., Pearson, N. J., Sharma, A. & Griffin, W. L. (1996). Quantitative analysis of trace elements in geological materials by laser ablation ICPMS: instrumental operating conditions and calibration values of NIST glasses. *Geostandard Newsletter* **20**, 247–261.
- O'Reilly, S. Y. & Griffin, W. L. (1988). Mantle metasomatism beneath Victoria, Australia I: metasomatic processes in Cr-diopside lherzolites. *Geochimica et Cosmochimica Acta* **52**, 433–447.
- O'Reilly, S. Y., Griffin, W. L. & Ryan, C. G. (1991). Residence of trace elements in metasomatized spinel lherzolite xenoliths: a proton-microprobe study. *Contributions to Mineralogy and Petrology* **109**, 98–113.
- Roden, M. F. & Shimizu, N. (1993). Ion microprobe analyses bearing on the composition of the upper mantle beneath the Basin and Range and Colorado Plateau Provinces. *Journal of Geophysical Research* **98**, 14091–14108.
- Roest, W. R., Dañobeita, J. J., Verhof, J. & Collette, B. J. (1992). Magnetic anomalies in the Canary Basin and the Mesozoic evolution of the central North Atlantic. *Marine Geophysical Research* **14**, 1–24.
- Rudnick, R. L., McDonough, W. F. & Orpin, A. (1994). Northern Tanzania peridotite xenoliths: a comparison with Kaapval peridotites and inferences on metasomatic reactions. In: Meyer, H. O. A. & Leonardos, O. (eds) *Kimberlites, Related Rocks and Mantle Xenoliths, Vol. 1. Proceedings of the 5th International Kimberlite Conference, Rio de Janeiro*. Rio de Janeiro: Companhia de Pesquisa de Recursos Minerais (CPRM), pp. 336–353.
- Salters, V. J. M. & Longhi, J. (1999). Trace element partitioning during the initial stages of melting beneath mid-ocean ridges. *Earth and Planetary Science Letters* **166**, 15–30.
- Salters, V. J. M. & Shimizu, N. (1988). World-wide occurrence of HFSE-depleted mantle. *Geochimica et Cosmochimica Acta* **52**, 2177–2182.
- Schmincke, H.-U. (1982). Volcanic and chemical evolution of the Canary Islands. In: von Rad, U., Hinz, K., Sarnthein, M. & Seibold, E. (eds) *Geology of the Northwest African Continental Margin*. Berlin: Springer, pp. 273–306.
- Siena, F., Beccaluva, L., Coltorti, M., Marchesi, S. & Morra, V. (1991). Ridge to hot-spot evolution of the Atlantic lithospheric mantle: evidence from Lanzarote peridotite xenoliths (Canary Islands). *Journal of Petrology, Special Lithosphere Issue* 271–290.
- Simonsen, S. L., Neumann, E.-R. & Seim, K. (2000). Sr–Nd–Pb isotope and trace element geochemistry of basaltic lavas in Tenerife: evidence for regional variations. *Journal of Volcanology and Geothermal Research* **103**, 299–312.
- Sisson, T. W. (1991). Pyroxene–high silica rhyolite trace element partition coefficients measured by ion microprobe. *Geochimica et Cosmochimica Acta* **55**, 1575–1585.
- Sweeney, R. J., Prozesky, V. & Przybyłowicz, W. (1995). Selected trace and minor element partitioning between peridotite minerals and carbonatite melts at 18–46 kb pressure. *Geochimica et Cosmochimica Acta* **59**, 3671–3683.
- Vannucci, R., Shimizu, N., Bottazzi, P., Ottolini, L., Piccardo, G. B. & Rampone, E. (1991). Rare earth and trace element geochemistry of clinopyroxenes from the Zabargad peridotite–pyroxenite association. *Journal of Petrology, Special Lherzolite Issue*, 255–269.
- Vannucci, R., Shimizu, N., Piccardo, G. B., Ottolini, L. & Bottazzi, P. (1993). Distribution of trace elements during breakdown of mantle

- garnet: an example from Zabargad. *Contributions to Mineralogy and Petrology* **113**, 437–449.
- Vannucci, R., Bottazzi, P., Wulff-Pedersen, E. & Neumann, E.-R. (1998). Naturally determined REE, Y, Sr, Zr and Ti partition coefficients between clinopyroxene and silicate melts under upper mantle conditions. *Earth and Planetary Science Letters* **158**, 39–51.
- Verhoef, J., Collette, B. J., Dañoibeita, J. J., Roeser, H. A. & Roest, W. R. (1991). Magnetic anomalies off West Africa (20–38°N). *Marine Geophysical Research* **13**, 81–103.
- Viti, C. & Frezzotti, M. L. (2002). Re-equilibration of glass and CO₂ inclusions in xenolith olivine: a TEM study. *American Mineralogist* **85**, 1390–1396.
- Whitehouse, M. J. & Neumann, E.-R. (1995). Sr–Nd–Pb isotope data for ultramafic xenoliths from Hierro, Canary Islands: melt infiltration processes in the upper mantle. *Contributions to Mineralogy and Petrology* **119**, 239–246.
- Wilson, M. & Guiraud, R. (1998). Late Permian to Recent magmatic activity on the African–Arabian margin of Tethys. In: MacGregor, D. S., Moody, R. T. J. & Clark-Lowes, D. D. (eds) *Petroleum Geology of North Africa*. Geological Society, London, *Special Publications* **132**, 231–263.
- Wood, B. J. (1979). A variably veined suboceanic upper mantle—genetic significance for mid-ocean ridge basalts from geochemical evidence. *Geology* **7**, 499–503.
- Wood, B. J. & Blundy, J. D. (1997). A predictive model for rare earth element partitioning between clinopyroxene and anhydrous silicate melt. *Contributions to Mineralogy and Petrology* **129**, 166–181.
- Woolley, A. R. & Kempe, D. R. C. (1989). Carbonatites: nomenclature, average chemical compositions, and element distribution. In: Bell, K. (ed.) *Carbonatites, Genesis and Evolution*. London: Unwin Hyman, pp. 1–14.
- Wulff-Pedersen, E., Neumann, E.-R. & Jensen, J. J. (1996). The upper mantle under La Palma, Canary Islands: formation of Si–K–Na-rich melt and its importance as a metasomatic agent. *Contributions to Mineralogy and Petrology* **125**, 113–139.
- Wulff-Pedersen, E., Neumann, E.-R., Vannucci, R., Bottazzi, P. & Ottolini, L. (1999). Silicic melts produced by reaction between peridotite and infiltrating basaltic melts: ion probe data on glasses and minerals in veined xenoliths from La Palma, Canary Islands. *Contributions to Mineralogy and Petrology* **137**, 59–82.
- Xu, X., O'Reilly, S. Y., Griffin, W. L. & Zhou, X. (2000). Genesis of young lithospheric mantle in southeastern China: an LAM-ICPMS trace element study. *Journal of Petrology* **41**, 111–148.
- Yaxley, G. M. & Green, D. H. (1996). Experimental reconstruction of sodic dolomitic carbonatite melts from metasomatised lithosphere. *Contributions to Mineralogy and Petrology* **124**, 359–364.
- Yaxley, G. M., Crawford, A. J. & Green, D. H. (1991). Evidence for carbonatite metasomatism in spinel peridotite xenoliths from western Victoria, Australia. *Earth and Planetary Science Letters* **107**, 305–317.
- Yaxley, G. M., Green, D. H. & Kamenetsky, V. (1998). Carbonate metasomatism in the southeastern Australian lithosphere. *Journal of Petrology* **39**, 1917–1930.
- Zhang, M., Stephenson, P. J., O'Reilly, S. Y., McCulloch, M. T. & Normann, M. (2001). Petrogenesis and geodynamic implications of late Cenozoic basalts in North Queensland, Australia: trace-element and Sr–Nd–Pb isotope evidence. *Journal of Petrology* **42**, 685–719.
- Zinngrube, E. & Foley, S. F. (1995). Metasomatism in mantle xenoliths from Gees, West Eifel, Germany: evidence for the genesis of calc alkaline glasses and metasomatic Ca-enrichment. *Contributions to Mineralogy and Petrology* **122**, 79–96.